Atomic L-shell Compton profiles and incoherent scattering factors: Theory*

Benjamin J. Bloch† and Lawrence B. Mendelsohn
Polytechnic Institute of Brooklyn, Brooklyn, New York 11201
(Received 19 June 1973)

Compton profiles are calculated for L-shell electrons within the Born approximation by use of nonrelativistic "exact" hydrogenic bound- and continuum-state wave functions. The wave functions are expressed in parabolic coordinates and the resulting matrix elements are evaluated following the method of F. Bloch (1934). Impulse-approximation profiles are calculated, and comparisons with the "exact" profiles show that, as expected, the two profiles lie very close to one another for weak binding and high incident photon energies. However, even when these conditions are not fulfilled, the two curves have a tendency to cross one another in the neighborhood of the profile center. This tendency has been observed in previous studies of K-shell profiles. However, unlike K-shell profiles, the $2S$ Compton profiles exhibit a secondary maximum. The secondary maxima occur at approximately the same region in q, where the impulse-approximation profiles exhibit a plateau. The location of this plateau is shown to be related to a node in the bound-state wave function and is around $q = Z/2$ for the $2S$ profiles. The impulse approximation, being a monotonic decreasing function in $|q|$, cannot exhibit the secondary-maximum structure appearing in the "exact" hydrogenic profiles. The intensity of the secondary maximum in the $2S$ profiles is reduced by over an order of magnitude from the central peak. The $2P^{(0)}$ Compton profiles also exhibit structure, however, unlike the relatively small secondary maximum in the $2S$, the two maxima in the $2P^{(0)}$ profiles are of the same order of magnitude. Integrated profiles (incoherent-scattering factors) are calculated and the impulse-approximation results agree with the "exact" results over a wide range of binding energies owing to profile crossover near the center. Waller-Hartree incoherent-scattering factors give a closer agreement with the "exact" results than observed for K-shell electrons; however, for low-momentum transfer the Waller-Hartree results can differ from "exact" results by more than 50%. In such regions, impulse-scattering factors represent a considerable improvement over the Waller-Hartree factors.

I. INTRODUCTION

There has been over the last few years, and especially in this last year, a resurgence of Compton-scattering measurements of the momentum distribution of atomic, molecular,[1,2,3] and solid-state systems.[4-9] These measurements, analyzed in a consistent fashion using theoretical core-electron Compton-profile calculations, can be utilized to study the momentum distributions of conduction-band electrons of conductors and semiconductors, the position of Fermi levels in these materials, the distribution of valence electrons in ionic solids, and correlation effects in free atoms and molecules. Simply stated, the outer electrons give the greatest contribution in the neighborhood of the Compton-profile center. Thus Compton scattering is a good way to study these electrons, which dominate most physical properties in atoms, molecules, and solids. The x-ray techniques themselves have acquired considerable sophistication over the past five years or so. Because of the large photoelectric absorption of Mo $K\alpha$ x-rays, the profile measurements have until recently been limited to systems with $Z \lesssim 13$. However, the development of Li-drifted germanium proportional detectors, which analyze γ-ray photons received, has led to a time gain of at least 300 over present x-ray techniques In addition, the higher energy of the γ rays makes some measurements on high-Z materials feasible, which are completely impractical at x-ray energies. Eisenberger and Reed[2] have stated that, "... all elements and their compounds can now be studied by Compton scattering..." using the γ-ray technique. There have been few calculations other than impulse-approximation calculations for elements with low Z, where many experimental x-ray profiles have been obtained. It is desirable to have accurate calculations for small atoms that are not only valid for large-momentum transfers but that are accurate for intermediate- and small-momentum transfers also, so as to study the domain of validity of the impulse approximation (IA). Hydrogenic one-electron calculations have been found to give quite accurate results for K- and L-shell photoelectric cross-section calculations.[10] One would expect that accurate Compton-profile calculations could also be obtained within this one-electron approximation for inner-shell electrons where the Coulomb attraction of the nucleus dominates.

Monte Carlo codes for x-ray and γ-ray penetration through materials are approaching the point

where improved values of the inelastic cross sections are called for over a wide range of momentum transfer. These codes have previously utilized either the Klein-Nishina scattering cross section (scattering from a free electron at rest) or the Klein-Nishina scattering cross section modified by the Waller-Hartree incoherent scattering factor. Since this factor is really an integrated (over angle) Compton profile, improved scattering factors can be obtained from more accurate profiles. For hydrogenic systems analytic "exact" profiles within the Born approximation have previously been obtained for K-shell electrons by Eisenberger and Platzman[11] and by Weiss.[12] Mendelsohn and Biggs[13] have calculated "exact" incoherent-scattering factors and impulse incoherent-scattering factors for K-shell electrons over a wide range of incident photon energies, scattering angles, and K-shell electron binding energies. It was demonstrated by them that the impulse-approximation K-shell scattering factors were much improved over Waller-Hartree results even for cases of strong binding and/or low incident photon energies. In the present work, a similar analysis for L-shell electrons shows this to be the case again. In addition, one can utilize the results and comparisons for both shells to obtain estimates of the improvement in accuracy of impulse incoherent-scattering factors over Waller-Hartree for real atoms. Additionally, some estimates of the inaccuracy incurred in using the Waller-Hartree factors in the present codes can be given.

Dumond[14] in 1929, in considering an atom with a momentum distribution of electrons, realized that such a distribution would cause Doppler broadening about the usual Compton-scattered wavelength λ_2^0. Considering the electrons to be free (but moving) before and after the collision, he found that the shift in scattered wavelength away from λ_2^0 the profile center, depends on the projection of $\vec{p}_1$, the original free-electron momentum before the collision, on the momentum transfer $\vec{k}$. He obtained the result:

$$\lambda_2 - \lambda_1 = (h/m_0c)[1 - \cos(2\theta)] - (\lambda^*/m_0c)q, \quad (1)$$

where

$$\lambda^* = (\lambda_1 \lambda_2)^{1/2} \sin\theta, \quad (2)$$

and

$$-q = (\vec{p}_1 \cdot \vec{k})/k. \quad (3)$$

λ_1 and λ_2 describe the incident and scattered photon wavelengths, respectively, while 2θ (rather than θ) represents the scattering angle. If $q = 0$ in Eq. (1), we have $\lambda_2 = \lambda_2^0$. For an atom with an isotropic momentum distribution, the intensity of the profile at a distance l from the center

$$l = \lambda_2 - \lambda_2^0 \quad (4)$$

should be proportional to the number of electrons with momentum p_1. This is under the assumption that scattering is equally probable from all values of momentum. Using this argument, Dumond found

$$\frac{d\sigma}{d\Omega dE} \sim J_{\text{imp}}(q) = \frac{1}{2}\int_q^\infty \frac{1}{p_1} |\chi(p_1)|^2 d^3p_1, \quad (5)$$

where $|\chi(p_1)|^2$ is the momentum probability distribution in the atom. Dumond's calculation is referred to as the impulse approximation (IA) and $J_{\text{imp}}(q)$ given by Eq. (5) is referred to as the Compton profile. The term "impulse" is used because the interaction between the photon and electron is assumed to take place so rapidly (large momentum transfers) that the electron does not see a variable potential during the interaction and can be treated as a free particle both before and after scattering. Calculations of $J_{\text{imp}}(q)$ for atoms and molecules with the use of hydrogenic and superposition of hydrogenic wave functions were made by Coulson and Duncanson.[15] More recently, Weiss, *et al.*[16] have calculated $J_{\text{imp}}(q)$, using the analytic Hartree-Fock wave functions of Clementi, for free atoms up to $Z = 32$. Mendelsohn, Biggs, and Mann[17] have recently calculated impulse profiles for the rare gases and certain select atoms through uranium using nonrelativistic and relativistic numerical Hartree-Fock wave functions. Also Benesch and Smith,[18] Brown and Smith,[19] and Eisenberger, Henneker and Cade,[20] have utilized more-accurate wave functions, including correlation, to calculate $J(q)$ for small atoms and molecules. In Be it was found that $J(q)$ decreased at $q = 0$ by about 5% below the Hartree-Fock result when a correlated wave function was used.

A more rigorous approach, considering the nonrelativistic Schrödinger equation, utilizing only the A^2 term in the perturbation (dropping $\vec{p} \cdot \vec{A}$ terms), and calculating the first-Born-approximation result, gives

$$\frac{d\sigma}{d\Omega dE} = \left(\frac{d\sigma}{d\Omega}\right)_T \left(\frac{E_2}{E_1}\right) \times \sum_f \left| \langle \psi_f | \sum_{j=1}^N e^{i\vec{k}\cdot\vec{r}_j} | \psi_i \rangle \right|^2 \delta(e_f - e_i - E), \quad (6)$$

where E_1, E_2 are the incident and scattered x-ray photon energies, respectively,

$$E = E_1 - E_2 = (e_f - e_i), \quad (7)$$

e_i, e_f are the initial and final electron energy, respectively; $\vec{k}$ is the momentum transfer

$$\vec{k} = \vec{k}_1 - \vec{k}_2, \tag{8a}$$

$$k^2 = k_1^2 + k_2^2 - 2k_1k_2\cos 2\theta; \tag{8b}$$

$k_i = E_i/\hbar c$; p is the final electron momentum; and ψ_i and ψ_f are the initial and final electron wave functions, respectively. The Thomson cross section is given by

$$\left(\frac{d\sigma}{d\Omega}\right)_T = \left(\frac{e^2}{m_0c^2}\right)^2 \frac{1}{2}(1+\cos^2 2\theta). \tag{9}$$

The δ function in Eq. (6) guarantees conservation of energy. It is only for a hydrogenic one-electron atom that Eq. (6) can be exactly evaluated analytically.

Considering a one-electron atom with nuclear charge Z, we make two approximations to regain the impulse approximation. First, the outgoing electron wave function ψ_f is taken to be a plane wave, and we take $e_f = p^2/2m_0$. Second, we take the bound-state energy $|e_i| = p_1^2/2m_0$, the energy associated with a freely moving electron. Choosing ψ_i as the usual hydrogenic bound-state wave function, one regains the impulse approximation in the form

$$\left(\frac{d\sigma}{d\Omega dE}\right)_{\text{imp}} \Big/ \left(\frac{d\sigma}{d\Omega}\right)_T = \frac{1}{Z}\ \frac{1}{27.212}\ \frac{n}{\kappa}\ \frac{E_2}{E_1}\ J_{\text{imp}}(q), \tag{10}$$

where n here is the principal quantum number of the ith state and

$$\kappa = (ka_0/Z)n \tag{11}$$

is a natural parameter for the problem. Equation (10) modifies Dumond's result with the slowly varying factor $(n/\kappa)(E_2/E_1)$. Still, such an approach does not shed much light on the accuracy or lack of it in the impulse approximation. Eisenberger and Platzman[11] used time-dependent operator perturbation theory, assuming violent interactions (short interaction times), to obtain the result of Eq. (10). In addition, comparing energy-transfer moments at fixed-momentum transfer of $(E_1/E_2)(d\sigma/d\Omega\, dE)$ for the impulse and for the exact hydrogenic atom, they showed that the first three moments with E^0, E^1, and E^2 agreed exactly; the fourth moment with E^3 evaluated in the impulse approximation differed from this moment evaluated for the exact system by terms of order κ^{-4}. Eisenberger and Platzman, using the matrix-element evaluation for the hydrogenic ground-state-to-continuum of Gummel and Lax,[21] have evaluated Eq. (6) exactly for the one-electron ground-state formulation. We refer to this as the "exact" (hydrogenic, nonrelativistic, first Born, $\vec{p}\cdot\vec{A}$ terms dropped) one-electron result (EH). Weiss[12] has compared the EH result with a calculation of Eq. (6), taking ψ_f as a plane wave. However, he treats ψ_i to be the correct hydrogenic bound-state wave function and e_i to be the exact binding energy. He finds poor agreement between the two profiles for 17.4 keV photons scattered through 160° with $Z=2$. The agreement becomes much worse with increasing binding (larger Z). He has also made some comparisons of impulse and exact profiles and found good agreement for $Z=2$ and 5 in the neighborhood of the profile center. Thus it is the effect of the two approximations (taking the potential energy entering the δ function to be zero, and assuming a plane wave for the outgoing electron) that leads to good agreement of the impulse with the "exact" one-electron result.

From a semiclassical treatment[22] it follows that inelastic scattering of an x-ray photon with energy E_1 into a scattering angle of 2θ from an atom in its ground state ψ_0 is described by the free-atom incoherent-scattering factor

$$S = \sum_{n>0}^{e_n = E_1 + e_0} \left(\frac{E_2}{E_1}\right)^2 \left|\langle \psi_n | \sum_{j=1}^{N} e^{i\vec{k}\cdot\vec{r}_j} | \psi_0 \rangle\right|^2, \tag{12}$$

with e_n, ψ_n representing a state of the atom, the sum including continuum terms; E_2 the energy of the scattered photon, where, as before, $E = E_1 - E_2 = e_n - e_0$. This factor S then enters the equation for the scattering cross section

$$\frac{d\sigma}{d\Omega} = S\left(\frac{d\sigma}{d\Omega}\right)_{\text{fr}}, \tag{13}$$

where $(d\sigma/d\Omega)_{\text{fr}}$ represents the scattering cross section for a free electron at rest, which, at low incident photon energies, is the Thomson cross section. Further approximations are then made in Eq. (12); setting $E_2 = E_1$, taking $e_n = \infty$, and taking $\vec{k} \neq \vec{k}(E_n)$. Closure is then employed to give the result[23]

$$S(\vec{k}) = \sum_{j,\lambda} \langle \psi_0 | e^{i\vec{k}\cdot(\vec{r}_j - \vec{r}_\lambda)} | \psi_0 \rangle - |F(\vec{k})|^2, \tag{14}$$

with

$$F(\vec{k}) = \sum_j \langle \psi_0 | e^{i\vec{k}\cdot\vec{r}_j} | \psi_0 \rangle, \tag{15}$$

the coherent-scattering factor. The calculation of $S(\vec{k})$ is thus reduced via Eq. (14) to a ground-state (two-particle) expectation value. Thomas-Fermi calculations of $S(\vec{k})$ given by Eq. (14) were originally performed by Bewilogua according to the formulation of Heisenberg. More recently, $S(\vec{k})$ has been calculated by utilization of numerical Hartree-Fock wave functions,[24,25] the Thomas-

Fermi-Dirac[13] model, and an alternative statistical model.[26] However, for strong binding, $(E_2/E_1)^2$ may be much less than 1, so that a more reasonable approximation to Eq. (12) is given by a suitable average of $(E_2/E_1)^2$ taken outside the sum. Thus in the work of Currat, DeCicco, and Weiss,[6] they define

$$S(\mathrm{WH}) = (E_2^0/E_1)^2 S, \tag{16}$$

where E_2^0 is employed to designate the usual Compton-scattering energy of a photon scattering from a free electron initially at rest, the (WH) represents Waller-Hartree. However, even Eq. (16) may give a large overestimate of the scattering in those cases where less than a half-profile remains, i.e., when $E_1 - e_0$, the largest possible value of E_2 for Compton scattering, is less than E_2^0. To illustrate this we have utilized Eq. (14) to evaluate incoherent-scattering factors S [and $S(\mathrm{WH})$] for one-electron ions with arbitrary Z in the form

$$S = 1 - |F|^2, \tag{17}$$

where $F = F(W)$, and

$$W = (\sin\theta/\lambda_1)(\text{Å}^{-1}); \tag{18}$$

W represents the momentum transfer in a perfectly elastic collision. This is consistent in utilizing Eq. (14) since E_2 is taken equal to E_1 in deriving it.

In addition to using Eq. (14), an alternative and direct method for finding the incoherent-scattering factor is to integrate Eq. (6) or Eq. (10) over energy

$$\begin{aligned} S &= \int_{|e_0|}^{E_1} \left(\frac{d\sigma}{d\Omega dE}\right) dE \Big/ \left(\frac{d\sigma}{d\Omega}\right)_T \\ &= \int_{|e_0|}^{E_1} \frac{dE\, n}{Z(27.212)\kappa} \left(\frac{E_2}{E_1}\right) J, \end{aligned} \tag{19}$$

where it is understood that subscripts will be used on the S and J to designate the impulse or the "exact" quantities.

II. GENERAL BLOCH RESULT

F. Bloch[27] in 1934, extending the theory of Wentzel,[28] used hydrogenic bound-state and continuum wave functions expressed in parabolic coordinates to evaluate the matrix elements in Eq. (6) for scattering from any initial hydrogenic bound state. The "exact" hydrogenic (EH) results were left in terms of residue integrals and derivatives, which were not evaluated because of their complexity. Bloch, in this nonrelativistic calculation, chose rather to approximate the general result at the onset and he then used this approximation to calculate the contribution to the Compton scattering of electrons in the different K- and L-shell orbitals. However, the expansion in powers of $(\mathfrak{K}a)^{-1}$ used by Bloch in deriving his approximate results, where $\mathfrak{K}$ is the final electron wave number and $a_0 \equiv \hbar^2/m_0e^2$, has been observed not to be a very good approximation for a $1S$ electron. As Eisenberger and Platzman have noted, under typical experimental conditions $(\mathfrak{K}a)^{-1}$ is not particularly small. Furthermore, Bloch's approximate K- and L-results, of use since 1934, have been shown by us and others to contain certain mathematical errors. We choose to return to his "exact" general result [Eq. (26) in Ref. 27] and evaluate the residue integrals, calculate the derivatives, and perform the necessary mathematics to derive analytic EH scattering formulas for the individual K- and L-shell electrons. The K-shell derivation, though yielding no new information, is presented here as a guide to illustrate the procedure used for obtaining the L-shell electronic results. We had previously attempted to derive the L-shell formulas by employing a procedure used by Gummel and Lax[21] to evaluate the K-shell matrix elements of Eq. (6), but the calculation proved too cumbersome.

A. Exact derivation

For a hydrogenlike atom with a single electron ($N=1$), and defining

$$I \equiv \left(\frac{d\sigma}{d\Omega dE}\right) \Big/ \left(\frac{d\sigma}{d\Omega}\right)_T, \tag{20}$$

Eq. (6) becomes

$$I = \frac{1}{(2\pi\hbar)^3} \left(\frac{E_2}{E_1}\right) \iint |M_{fi}|^2\, d\Omega\, p^2\, dp\, \delta(e_f - e_i - E), \tag{21}$$

where the scattering matrix has been defined as

$$|M_{fi}|^2 \equiv |\langle \psi_f | e^{i\vec{\mathfrak{k}}\cdot\vec{r}} | \psi_i \rangle|^2. \tag{22}$$

Taking a slight change of variables, and writing $e_f = p^2/2m_0$ for the final-electron energy, Eq. (21) assumes the form

$$\begin{aligned} I = \frac{(2m_0)^{3/2}}{(2\pi)^3\hbar^3} \left(\frac{E_2}{E_1}\right) \iint |M_{fi}|^2\, d\Omega \\ \times \left(\frac{p}{(2m_0)^{1/2}}\right) d\left(\frac{p^2}{2m_0}\right) \delta\left(\frac{p^2}{2m_0} - e_i - E\right). \end{aligned} \tag{23}$$

The δ-function properties may then be employed to perform one of the integrations, yielding

$$I = \frac{m_0 p}{2\pi^2\hbar^3} \left(\frac{E_2}{E_1}\right) \int |M_{fi}|^2\, d\Omega, \tag{24}$$

where

$$p = [2m_0(E + e_i)]^{1/2}. \tag{25}$$

We will express our results in terms of the final-electron wave number $\mathcal{K}$, thus writing $p=\hbar\mathcal{K}$; Eq. (24) then becomes

$$I=\frac{m_0\mathcal{K}}{2\pi^2\hbar^2}\left(\frac{E_2}{E_1}\right)\int|M_{fi}|^2\,d\Omega. \tag{26}$$

Going to parabolic coordinates and writing the final (continuum) wave function in terms of well-known contour integrals, Eq. (26) becomes

$$I=\frac{m_0}{\hbar^2\mathcal{K}}\left(\frac{E_2}{E_1}\right)\int_{-\infty}^{\infty}|\epsilon_{nla,\mathcal{K}m}(k)|^2\,dm, \tag{27}$$

where

$$\epsilon_{nla,\mathcal{K}m}(k)\equiv\frac{\pi}{2}\int U_{\mathcal{K}ma}U_{nla}\,e^{i(k/2\mathcal{K})(\xi-\eta)}(\xi+\eta)\,d\eta\,d\xi \tag{28}$$

Here the initial and final wave functions are given by U_{nla} and $U_{\mathcal{K}ma}$, respectively; a is the azimuthal quantum number of the initial state; m is a parabolic quantum number related to the direction of momentum of the recoil electron; and ξ,η are the usual parabolic coordinates.

The form of Eq. (27) is the same as Eq. (19) in Bloch's paper, except that he did not include the factor E_2/E_1. Following Bloch, $\epsilon_{nla,\mathcal{K}m}(k)$ can be evaluated as

$$\epsilon_{nla,\mathcal{K}m}(k)=\pi^{3/2}(-1)^l\,2^{-3-l}(A_{nla})^{1/2}\times\frac{\partial^{n-l-1}}{\partial t^{n-l-1}}\,q_{la}\big|_{t=0}, \tag{29}$$

where A_{nla} is the normalization constant related to the bound-state wave function and defining $\alpha\equiv 2Zm_0e^2/n\hbar^2$ and $\beta\equiv Zm_0e^2/2\hbar^2\mathcal{K}$, we get

$$\begin{aligned}q_{la}(\mathcal{K},m,k,t)=(i\mathcal{K})^{-2a}\,\frac{\alpha^l}{2^{l-a}}\,C_{\mathcal{K}ma}\,\frac{(-1)^{2l+1}}{(1-t)^{2l+2}}\lim_{\substack{\mu_1\to0\\ \mu_2\to0}}\sum_{j=0}^{l-a}c_j\Bigg\{\left(\frac{\partial}{\partial\mu_1}+\frac{\partial}{\partial\mu_2}\right)^{1+l-a-j}\\ \times\left(\frac{\partial}{\partial\mu_1}-\frac{\partial}{\partial\mu_2}\right)^{j}\frac{\partial^{2a}}{\partial\mu_1^a\,\partial\mu_2^a}\left[\frac{\alpha}{4}\left(\frac{1+t}{1-t}\right)-\mu_1-i\left(\frac{k-\mathcal{K}}{2}\right)\right]^{(a-1)/2+i(\beta+m)}\\ \times\left[\frac{\alpha}{4}\left(\frac{1+t}{1-t}\right)-\mu_1-i\left(\frac{k+\mathcal{K}}{2}\right)\right]^{(a-1)/2-i(\beta+m)}\left[\frac{\alpha}{4}\left(\frac{1+t}{1-t}\right)-\mu_2+i\left(\frac{k+\mathcal{K}}{2}\right)\right]^{(a-1)/2+i(\beta-m)}\\ \times\left[\frac{\alpha}{4}\left(\frac{1+t}{1-t}\right)-\mu_2+i\left(\frac{k-\mathcal{K}}{2}\right)\right]^{(a-1)/2-i(\beta-m)}\Bigg\},\end{aligned} \tag{30}$$

where $C_{\mathcal{K}ma}$ is the normalization constant of the continuum wave function and the quantities c_j are certain numbers defining the spherical harmonics P_l^a; thus

$$P_l^a(\cos2\theta)=(1-\cos^2 2\theta)^{a/2}\sum_{j=0}^{l-a}c_j\cos^j 2\theta. \tag{31}$$

For purposes of completeness, the derivation of this result is detailed in Appendix B, together with expressions for the constants A_{nla} and $C_{\mathcal{K}ma}$.

B. "Exact" K-shell derivation

For a 1S electron, $n=1$, $l=0$, $j=0$, $c_0=1$. Thus Eq. (30) becomes

$$\begin{aligned}q_{00}(\mathcal{K},m,k,0)=C_{\mathcal{K}m0}\lim_{\substack{\mu_1\to0\\ \mu_2\to0}}\Bigg[\left(\frac{\partial}{\partial\mu_1}+\frac{\partial}{\partial\mu_2}\right)\left(\frac{\alpha}{4}-\mu_1-i\,\frac{\alpha}{4\gamma}\right)^{-1/2-i(\beta+m)}\\ \times\left(\frac{\alpha}{4}-\mu_2+i\,\frac{\alpha}{4\gamma}\right)^{-1/2+i(\beta-m)}\left(\frac{\alpha}{4}-\mu_1-i\,\frac{\alpha v}{4}\right)^{-1/2+i(\beta+m)}\\ \times\left(\frac{\alpha}{4}-\mu_2+i\,\frac{\alpha v}{4}\right)^{-1/2-i(\beta-m)}\Bigg],\end{aligned} \tag{32}$$

where

$$1/\gamma\equiv 2(k+\mathcal{K})/\alpha,\quad v\equiv(2/\alpha)(k-\mathcal{K}), \tag{33}$$

and

$$C_{\mathcal{K}m0}=\tfrac{1}{2}\pi^{-3/2}\mathcal{K}e^{\pi\beta}\,|\Gamma[\tfrac{1}{2}+i(\beta+m)]|\,|\Gamma[\tfrac{1}{2}+i(\beta-m)]|. \tag{34}$$

Writing

$$\Gamma_0\equiv(\tfrac{1}{4}\alpha)^{-2}(1-iv)^{-1/2+i(\beta+m)}(1-i/\gamma)^{-1/2-i(\beta+m)}(1+i/\gamma)^{-1/2+i(\beta-m)}(1+iv)^{-1/2-i(\beta-m)}, \tag{35}$$

Eq. (32) becomes, after a little algebra,

$$q_{00}(\mathfrak{K}, m, k, 0) = C_{\mathfrak{K}m0}\,\Gamma_0(\tfrac{1}{4}\alpha)^{-1}\left(\frac{-1-2\beta v+2im}{1+v^2}+\frac{-1+2\beta/\gamma-2im}{1+1/\gamma^2}\right). \tag{36}$$

Inserting the expression for $C_{\mathfrak{K}m0}$ and simplifying Γ_0, Eq. (36) becomes

$$q_{00}(\mathfrak{K}, m, k, 0) = 2\frac{a_0^2}{Z^2}\mathfrak{K}^2 k\left(\frac{\alpha}{4}\right)^{-3}\pi^{-3/2}e^{\pi\beta}\,|\,\Gamma[\tfrac{1}{2}+i(\beta+m)]\,|\,|\,\Gamma[\tfrac{1}{2}+i(\beta-m)]\,|$$
$$\times\left(2im-\frac{k}{\mathfrak{K}}\right)(1+v^2)^{-3/2+im}\left(1+\frac{1}{\gamma^2}\right)^{-3/2-im}\exp\left(-2\beta\tan^{-1}\frac{2(\gamma+v)(1-\gamma v)}{4v\gamma+(1-v^2)(\gamma^2-1)}\right). \tag{37}$$

Thus inserting this value in Eq. (29) and taking the absolute value squared, we obtain

$$|\epsilon_{100,\mathfrak{K}m}(k)|^2 = (2Z)^{-4}A_{100}\mathfrak{K}^4a_0^4k^2\left(\frac{\alpha}{4}\right)^{-6}e^{2\pi\beta}\,|\,\Gamma[\tfrac{1}{2}+i(\beta+m)]\,|^2\,|\,\Gamma[\tfrac{1}{2}+i(\beta-m)]\,|^2$$
$$\times(1+v^2)^{-3}\left(1+\frac{1}{\gamma^2}\right)^{-3}\left[4m^2+\left(\frac{\kappa}{\mathfrak{K}}\right)^2\right]\exp\left(-4\beta\tan^{-1}\frac{2(\gamma+v)(1-\gamma v)}{4v\gamma+(1-v^2)(\gamma^2-1)}\right). \tag{38}$$

Using the relationship

$$|\,\Gamma(\tfrac{1}{2}+iy)\,|^2 = \pi/\cosh\pi y \tag{39}$$

and

$$e^{2\pi\beta}\,|\,\Gamma[\tfrac{1}{2}+i(\beta+m)]\,|^2\,|\,\Gamma[\tfrac{1}{2}+i(\beta-m)]\,|^2 = \frac{\pi^2e^{2\pi\beta}}{\cosh\pi(\beta+m)\cosh\pi(\beta-m)}$$
$$= \frac{4\pi^2}{(1+e^{-2\pi(\beta+m)})(1+e^{-2\pi(\beta-m)})} \tag{40}$$

Eq. (38) becomes

$$|\epsilon_{100,\mathfrak{K}m}(k)|^2 = 16\pi^2A_{100}\left(\frac{\alpha}{2}\right)^{-6}\mathfrak{K}^4\left(\frac{a_0}{Z}\right)^4k^2(1+v^2)^{-3}\left(1+\frac{1}{\gamma^2}\right)^{-3}$$
$$\times\left(\frac{4m^2+(k/\mathfrak{K})^2}{(1+e^{-2\pi(\beta+m)})(1+e^{-2\pi(\beta-m)})}\right)\exp\left(-4\beta\tan^{-1}\frac{2(\gamma+v)(1-\gamma v)}{4v\gamma+(1-v^2)(\gamma^2-1)}\right). \tag{41}$$

We now have to integrate this expression over m, and defining

$$|\epsilon_{100,\mathfrak{K}}(k)|^2 \equiv \int_{-\infty}^{\infty}|\epsilon_{100,\mathfrak{K}m}(k)|^2\,dm, \tag{42}$$

Eq. (27) becomes

$$I = \frac{m_0}{\hbar^2\mathfrak{K}}\left(\frac{E_2}{E_1}\right)16\pi^2A_{100}\left(\frac{\alpha}{2}\right)^{-6}\mathfrak{K}^4\left(\frac{a_0}{Z}\right)^4k^2(1+v^2)^{-3}\left(1+\frac{1}{\gamma^2}\right)^{-3}$$
$$\times\exp\left(-4\beta\tan^{-1}\frac{2(\gamma+v)(1-\gamma v)}{4\gamma v+(1-v^2)(\gamma^2-1)}\right)\int_{-\infty}^{\infty}\frac{4m^2+(k/\mathfrak{K})^2}{(1+e^{-2\pi(\beta+m)})(1+e^{-2\pi(\beta-m)})}\,. \tag{43}$$

Now

$$\int_{-\infty}^{\infty}\frac{dm}{(1+e^{-2\pi(\beta+m)})(1+e^{-2\pi(\beta-m)})} = 2\beta(1-e^{-4\pi\beta})^{-1} \tag{44}$$

and

$$\int_{-\infty}^{\infty}\frac{m^2\,dm}{(1+e^{-2\pi(\beta+m)})(1+e^{-2\pi(\beta-m)})} = \tfrac{1}{6}\beta(1+4\beta^2)(1-e^{-4\pi\beta})^{-1}. \tag{45}$$

The detailed evaluation of these integrals is contained in Appendix C.

Defining $\kappa \equiv nka_0/Z$ and $P \equiv n\mathfrak{K}a_0/Z$, these quantities assume the values for K-shell electrons ($n=1$), $\kappa = ka_0/Z$ and $P = \mathfrak{K}a_0/Z$. Here A_{100} becomes

$$A_{100} = 2\alpha^3/\pi^2,$$

where $\alpha = 2Z/a_0$, and thus Eq. (43) becomes, with these substitutions and definitions,

$$I = \frac{256 m_0 a_0^2 \kappa^2}{3\hbar^2 Z^2}\left(\frac{E_2}{E_1}\right)(1-e^{-2\pi/P})^{-1}\frac{1+3\kappa^2+P^2}{[(1+\kappa^2-P^2)^2+4P^2]^3}\exp\left(-\frac{2}{P}\tan^{-1}\frac{2P}{1+\kappa^2-P^2}\right). \tag{46}$$

This result is the same as derived by Eisenberger and Platzman[11] using the matrix evaluation by Gummel and Lax.[21]

We now go over to atomic units, whereby

$$m_0 a_0^2/\hbar^2 = 1/27.212,$$

yielding

$$I \equiv I_{1S}^{\text{exact}} = \frac{256\kappa^2}{3\times 27.212 Z^2}\left(\frac{E_2}{E_1}\right)(1-e^{-2\pi/P})^{-1}\frac{1+3\kappa^2+P^2}{[(1+\kappa^2-P^2)^2+4P^2]^3}\exp\left(-\frac{2}{P}\tan^{-1}\frac{2P}{1+\kappa^2-P^2}\right). \tag{47}$$

The Compton profile is given by

$$J_{1S}^{\text{exact}} = (E_1/E_2)27.212\kappa Z I_{1S}^{\text{exact}}. \tag{48}$$

Thus Eq. (48) becomes

$$J_{1S}^{\text{exact}} = \frac{256\kappa^3}{3Z}(1-e^{-2\pi/P})^{-1}\frac{1+3\kappa^2+P^2}{[(1+\kappa^2-P^2)^2+4P^2]^3}\exp\left(-\frac{2}{P}\tan^{-1}\frac{2P}{1+\kappa^2-P^2}\right). \tag{49}$$

III. DERIVATION OF "EXACT" L-SHELL PROFILES

A. 2S EH Compton profile

For this case $n=0$, $l=0$, $a=0$, $j=0$ and Eq. (30) becomes, setting $T \equiv (1+t)/(1-t)$,

$$\begin{aligned} q_{00}(\mathfrak{K}, m, k, T) = (\tfrac{1}{4}\alpha)^{-3} C_{\mathfrak{K}m0}[(1+T)^4/4][(T-iv)^{-1/2+i(\beta+m)}(T+iv)^{-1/2-i(\beta-m)}(T-i/\gamma)^{-1/2-i(\beta+m)} \\ \times (T+i/\gamma)^{-1/2+i(\beta-m)}] \\ \times\{(T-iv)^{-1}[-\tfrac{1}{2}+i(\beta+m)]+(T-i/\gamma)^{-1}[-\tfrac{1}{2}-i(\beta+m)]+(T+iv)^{-1} \\ \times[-\tfrac{1}{2}-i(\beta-m)]+[-\tfrac{1}{2}+i(\beta-m)](T+i/\gamma)^{-1}\}. \end{aligned} \tag{50}$$

Defining

$$\mu_1 \equiv -\tfrac{1}{2}+i(\beta+m),\quad \mu_2 \equiv -\tfrac{1}{2}-i(\beta-m),\quad \mu_3 \equiv -\tfrac{1}{2}+i(\beta-m),\quad \mu_4 \equiv -\tfrac{1}{2}-i(\beta+m), \tag{51}$$

we obtain

$$\begin{aligned} q_{00}(\mathfrak{K}, m, k, T) = (\tfrac{1}{4}\alpha)^{-3} C_{\mathfrak{K}m0}[(1+T)^2/4][(T-iv)^{\mu_1}(T+iv)^{\mu_2}(T-i/\gamma)^{\mu_4}(T+i/\gamma)^{\mu_3}] \\ \times[\mu_1(T-iv)^{-1}+\mu_4(T-i/\gamma)^{-1}+\mu_2(T+iv)^{-1}+\mu_3(T+i/\gamma)^{-1}]. \end{aligned} \tag{52}$$

Since we have set $T=(1+t)/(1-t)$, Eq. (29) becomes

$$\epsilon_{200,\mathfrak{K}m}(k) = \pi^{3/2}2^{-2}(A_{200})^{1/2}\left.\frac{\partial q_{00}(\mathfrak{K}, m, k, T)}{\partial T}\right|_{T=1}, \tag{53}$$

and we must therefore calculate $\partial q_{00}(\mathfrak{K}, m, k, T)/\partial T$ and then evaluate at $T=1$ (corresponding to $t=0$). Differentiating Eq. (52) with respect to T, we get

$$\begin{aligned} \frac{\partial q_{00}(\mathfrak{K}, m, k, T)}{\partial T} = (\tfrac{1}{4}\alpha)^{-3} C_{\mathfrak{K}m0}\left(\frac{1+T}{2}\right)\left[(T-iv)^{\mu_1}(T+iv)^{\mu_2}\left(T-\frac{i}{\gamma}\right)^{\mu_4}\left(T+\frac{i}{\gamma}\right)^{\mu_3}\right] \\ \times\left\{\left[\mu_1(T-iv)^{-1}+\mu_4\left(T-\frac{i}{\gamma}\right)^{-1}+\mu_2(T+iv)^{-1}+\mu_3\left(T+\frac{i}{\gamma}\right)^{-1}\right]\right. \\ +\left(\frac{1+T}{2}\right)\left[-\mu_1(T-iv)^{-2}-\mu_4\left(T-\frac{i}{\gamma}\right)^{-2}-\mu_2(T+iv)^{-1}-\mu_3\left(T+\frac{i}{\gamma}\right)^{-2}\right] \\ \left.+\left(\frac{1+T}{2}\right)\left[\mu_1(T-iv)^{-1}+\mu_4\left(T-\frac{i}{\gamma}\right)^{-1}+\mu_2(T+iv)^{-1}+\mu_3\left(T+\frac{i}{\gamma}\right)^{-1}\right]\right\}, \end{aligned} \tag{54}$$

Now let

$$A \equiv 1 + iv, \quad B \equiv 1 + v^2 = AA^*, \quad C \equiv 1 + i/\gamma, \quad D \equiv 1 + 1/\gamma^2 = CC^*. \tag{55}$$

At this point care must be taken to ensure that the constants used reflect their proper values for the 2S case. Thus in this case α ($n=2$) has the value

$$\alpha = Z m_0 e^2/\hbar^2. \tag{56}$$

Consequently we now set

$$2a_0 k \equiv \kappa, \quad 2a_0 \mathfrak{K} \equiv P,$$

so that (57)

$$v = \kappa - P, \quad 1/\gamma = \kappa + P.$$

With these substitutions and some algebra, Eq. (54) becomes

$$\begin{aligned}\left.\frac{\partial q_{00}(\mathfrak{K}, m, k, T)}{\partial T}\right|_{T=1} &= \left(\frac{\alpha}{4}\right)^{-3} C_{\mathfrak{K}m0} B^{-3/2+im} D^{-3/2-im} \exp\left(-2\beta \tan^{-1}\frac{2P}{1+\kappa^2-P^2}\right) \\ &\times \left(2im\left[D - B + 4\beta\left(v + \frac{1}{\gamma}\right) - \frac{D}{B}(3 - v^2 + 4\beta v) + \frac{B}{D}\left(3 - \frac{1}{\gamma^2} - \frac{4\beta}{\gamma}\right)\right]\right. \\ &+ \left\{-4m^2\left(\frac{D}{B} + \frac{B}{D} - 2\right) - 2(1+2\beta v)\left(-1 + \frac{2\beta}{\gamma}\right) - D(1+2\beta v) + B\left(-1 + \frac{2\beta}{\gamma}\right)\right. \\ &\left.\left. + \frac{D}{B}[1 - v^2 + 4\beta v + (1+2\beta v)^2] + \frac{B}{D}\left[1 - \frac{1}{\gamma^2} - \frac{4\beta}{\gamma} + \left(-1 + \frac{2\beta}{\gamma}\right)^2\right]\right\}\right).\end{aligned} \tag{58}$$

$C_{\mathfrak{K}m\alpha}$ takes on the value,

$$C_{\mathfrak{K}m0} = (PZ/4a_0)\, \pi^{-3/2} e^{\pi\beta} |\Gamma[\tfrac{1}{2} + i(\beta + m)]| \, |\Gamma[\tfrac{1}{2} + i(\beta - m)]|. \tag{59}$$

Substituting Eqs. (58) and (59) into Eq. (53), and taking the square of the absolute value, leads to

$$\begin{aligned}|\epsilon_{200,\mathfrak{K}m}(k)|^2 &= A_{200}\left(\frac{\alpha}{4}\right)^{-6} \frac{P^2 Z^2}{64 a_0^2} e^{2\pi\beta} |\Gamma[\tfrac{1}{2} + i(\beta + m)]|^2 \, |\Gamma[\tfrac{1}{2} + i(\beta - m)]|^2 \\ &\times \left\{m^2 R_1^2 + \left[-2m^2\left(\frac{D}{B} + \frac{B}{D} - 2\right) + R_2\right]^2\right\} B^{-3} D^{-3} \exp\left(-4\beta \tan^{-1}\frac{2P}{1+\kappa^2-P^2}\right),\end{aligned} \tag{60}$$

where we have defined

$$\begin{aligned}R_1 &\equiv D - B + 4\beta\left(v + \frac{1}{\gamma}\right) - \frac{D}{B}(3 - v^2 + 4\beta v) + \frac{B}{D}\left(3 - \frac{1}{\gamma^2} - \frac{4\beta}{\gamma}\right), \\ R_2 &\equiv \frac{1}{2}\left\{-2(1 + 2\beta v)\left(-1 + \frac{2\beta}{\gamma}\right) - D(1 + 2\beta v) + B\left(-1 + \frac{2\beta}{\gamma}\right)\right. \\ &\left. + \frac{D}{B}[(1+2\beta v)^2 + 4\beta v + 1 - v^2] + \frac{B}{D}\left[\left(-1 + \frac{2\beta}{\gamma}\right)^2 - \frac{4\beta}{\gamma} + 1 - \frac{1}{\gamma^2}\right]\right\}.\end{aligned} \tag{61}$$

As in the 1S case we are interested in the integral of Eq. (60) over all m, thus

$$\begin{aligned}|\epsilon_{200}(k)|^2 &\equiv \int_{-\infty}^{\infty} |\epsilon_{200,\mathfrak{K}m}(k)|^2 \, dm \\ &= A_{200}(\tfrac{1}{4}\alpha)^{-6} \frac{\pi^2 P^2 Z^2}{16 a_0^2} B^{-3} D^{-3} \exp\left(-4\beta \tan^{-1}\frac{2P}{1+\kappa^2-P^2}\right) \\ &\times \left[R_2^2 \int_{-\infty}^{\infty} \frac{dm}{(1 + e^{-2\pi(\beta+m)})(1 + e^{-2\pi(\beta-m)})}\right. \\ &+ (R_1^2 - 4R_2)\left(\frac{D}{B} + \frac{B}{D} - 2\right) \int_{-\infty}^{\infty} \frac{m^2\, dm}{(1 + e^{-2\pi(\beta+m)})(1 + e^{-2\pi(\beta-m)})} \\ &\left. + 4\left(\frac{D}{B} + \frac{B}{D} - 2\right)^2 \int_{-\infty}^{\infty} \frac{m^4\, dm}{(1 + e^{-2\pi(\beta+m)})(1 + e^{-2\pi(\beta-m)})}\right].\end{aligned} \tag{62}$$

The first two integrals have been evaluated for the 1S case [see Eqs. (44) and (45)], and the third integral (see Appendix C for details) has the value

$$\int_{-\infty}^{\infty} \frac{m^4\,dm}{(1+e^{-2\pi(\beta+m)})(1+e^{-2\pi(\beta-m)})} = \frac{\beta}{5}\left(\frac{7}{24}+\frac{5\beta^2}{3}+2\beta^4\right)(1-e^{-4\pi\beta})^{-1}. \tag{63}$$

Going over to atomic units we arrive at the final result

$$\begin{aligned} I \equiv I_{2S}^{\text{exact}} &= \frac{2^8}{27.212Z^2}\left(\frac{E_2}{E_1}\right) B^{-3}D^{-3}(1-e^{-4\pi/P})^{-1} \\ &\times\left\{2R_2^2+\frac{1+4/P^2}{6}\left[R_1^2-4R_2\left(\frac{D}{B}+\frac{B}{D}-2\right)\right]+\frac{4}{5}\left(\frac{D}{B}+\frac{B}{D}-2\right)^2\left(\frac{7}{24}+\frac{5}{3P^2}+\frac{2}{P^4}\right)\right\} \\ &\times\exp\left(-\frac{4}{P}\tan^{-1}\frac{2P}{1+\kappa^2-P^2}\right), \end{aligned} \tag{64}$$

where

$$\begin{aligned} R_1 &\equiv D-B+\frac{4}{P}\left(v+\frac{1}{\gamma}\right)-\frac{D}{B}\left(3-v^2+\frac{4v}{P}\right)+\frac{B}{D}\left(3-\frac{1}{\gamma^2}-\frac{4}{\gamma P}\right), \\ R_2 &\equiv \frac{1}{2}\left\{-2\left(1+\frac{2v}{P}\right)\left(-1+\frac{2}{\gamma P}\right)-D\left(1+\frac{2v}{P}\right)+B\left(-1+\frac{2}{\gamma P}\right)\right. \\ &\left.+\frac{D}{B}\left[1-v^2+\frac{4v}{P}+\left(1+\frac{2v}{P}\right)^2\right]+\frac{B}{D}\left[1-\frac{1}{\gamma^2}-\frac{4}{\gamma P}+\left(-1+\frac{2}{\gamma P}\right)^2\right]\right\}. \end{aligned} \tag{65}$$

The Compton profile is then given by

$$J_{2S}^{\text{exact}} = (E_1/E_2)\,13.606\,\kappa Z\, I_{2S}^{\text{exact}}. \tag{66}$$

B. $2P^{(0)}$ EH Compton profile

For this case $n=2$, $l=1$, $a=0$ and from Eq. (31), $c_0=0$ and $c_1=1$, $j=1$. Thus Eq. (30) becomes

$$\begin{aligned} q_{10}(\mathfrak{K},m,k,0) &= -C_{\mathfrak{K}m0}\,\frac{\alpha}{2}\lim_{\substack{\mu_1\to 0\\ \mu_2\to 0}}\left(\frac{\partial}{\partial\mu_1}+\frac{\partial}{\partial\mu_2}\right)\left(\frac{\partial}{\partial\mu_1}-\frac{\partial}{\partial\mu_2}\right) \\ &\times\left[\left(\frac{\alpha}{4}-\mu_1-i\,\frac{k-\mathfrak{K}}{2}\right)^{-1/2+i(\beta+m)}\left(\frac{\alpha}{4}-\mu_1-i\,\frac{k+\mathfrak{K}}{2}\right)^{-1/2-i(\beta+m)}\right. \\ &\left.\times\left(\frac{\alpha}{4}-\mu_2+i\,\frac{k+\mathfrak{K}}{2}\right)^{-1/2+i(\beta-m)}\left(\frac{\alpha}{4}-\mu_2+i\,\frac{k-\mathfrak{K}}{2}\right)^{-1/2-i(\beta-m)}\right], \end{aligned} \tag{67}$$

while Eq. (29) becomes

$$\epsilon_{210,\mathfrak{K}m}(k) = -\pi^{3/2}2^{-4}(A_{210})^{1/2}\,q_{10}(\mathfrak{K},m,k,0). \tag{68}$$

Making use of

$$\left(\frac{\partial}{\partial\mu_1}+\frac{\partial}{\partial\mu_2}\right)\left(\frac{\partial}{\partial\mu_1}-\frac{\partial}{\partial\mu_2}\right) \equiv \frac{\partial^2}{\partial\mu_1^2}-\frac{\partial^2}{\partial\mu_2^2},$$

and

$$v=(2/\alpha)(k-\mathfrak{K}),\quad 1/\gamma=(2/\alpha)(k+\mathfrak{K}),$$

with the definition in Eq. (56), we note, taking the limits $\mu_1\to 0$ and $\mu_2\to 0$, that Eq. (67) becomes, after some lengthy algebra,

$$q_{10}(\mathfrak{K},m,k,0) = -C_{\mathfrak{K}m0}\left(\frac{\alpha}{4}\right)^{-4}\left(\frac{\alpha}{2}\right)B^{-1/2+im}D^{-1/2-im}\exp\left(-2\beta\tan^{-1}\frac{2P}{1+\kappa^2-P^2}\right)[4mR_1+i(R_3+4m^2R_2)], \tag{69}$$

where

$$R_1 \equiv \frac{2\beta(1-v/\gamma)}{BD} + \frac{1}{B^2}[2v-\beta(1-v^2)] + \frac{1}{D^2}\left[-\frac{2}{\gamma} - \beta\left(1-\frac{1}{\gamma^2}\right)\right],$$

$$R_2 \equiv \frac{v+1/\gamma}{BD} - \left(\frac{v}{B^2} + \frac{1}{\gamma D^2}\right),$$

$$R_3 \equiv \frac{(1+4\beta^2)(v+1/\gamma)}{BD} + \frac{1}{B^2}[v(3-4\beta^2) - 4\beta(1-v^2)] + \frac{1}{D^2}\left[\frac{1}{\gamma}(3-4\beta^2) + 4\beta\left(1-\frac{1}{\gamma^2}\right)\right], \tag{70}$$

$$B \equiv 1+v^2, \quad D \equiv 1+1/\gamma^2.$$

Substituting Eqs. (69) and (59) into Eq. (68), taking the square of the absolute value and integrating over m, and making use of the integrals evaluated previously for the 2S case, the final result in atomic units is

$$I \equiv I^{\text{exact}}_{2P(0)} = \frac{128}{27.212Z^2}\left(\frac{E_2}{E_1}\right)\frac{1}{BD}(1-e^{-4\pi/P})^{-1}\left[\frac{8}{5}R_2^2\left(\frac{7}{24}+\frac{5}{3P^2}+\frac{2}{P^4}\right)+\frac{2}{3}\left(1+\frac{4}{P^2}\right)(2R_1^2+R_2R_3)+R_3^2\right]$$

$$\times\exp\left(-\frac{4}{P}\tan^{-1}\frac{2P}{1+\kappa^2-P^2}\right), \tag{71}$$

$$R_1 \equiv \frac{(2/P)(1-v/\gamma)}{BD} + \frac{1}{B^2}\left[2v - \frac{1}{P}(1-v^2)\right] + \frac{1}{D^2}\left[-\frac{2}{\gamma} - \frac{1}{P}\left(1-\frac{1}{\gamma^2}\right)\right],$$

$$R_2 \equiv \frac{(v+1/\gamma)}{BD} - \left(\frac{v}{B^2} + \frac{1}{\gamma D^2}\right), \tag{72}$$

$$R_3 \equiv \frac{(1+4/P^2)(v+1/\gamma)}{BD} + \frac{1}{B^2}\left[v\left(3-\frac{4}{P^2}\right) - \frac{4}{P}(1-v^2)\right] + \frac{1}{D^2}\left[\frac{1}{\gamma}\left(3-\frac{4}{P^2}\right) + \frac{4}{P}\left(1-\frac{1}{\gamma^2}\right)\right].$$

The Compton profile is then given by

$$J^{\text{exact}}_{2P(0)} = (E_1/E_2)\,13.606\kappa Z I^{\text{exact}}_{2P(0)}. \tag{73}$$

C. $2P^{(\pm1)}$ EH Compton profile

The $2P^{(+1)}$ and $2P^{(-1)}$ give the same result and here we have $n=2$, $l=1$, $a=1$, $c_0=1$, $j=0$. Thus Eq. (79) becomes

$$\epsilon_{211,\mathfrak{K}m}(k) = -\pi^{3/2}2^{-4}(A_{211})^{1/2}q_{11}(\mathfrak{K}, m, k, 0), \tag{74}$$

while Eq. (30) takes on the value

$$q_{11}(\mathfrak{K}, m, k, 0) = \alpha\mathfrak{K}^{-2}C_{\mathfrak{K}m1}\lim_{\substack{\mu_1\to 0\\ \mu_2\to 0}}\left(\frac{\partial}{\partial\mu_1}+\frac{\partial}{\partial\mu_2}\right)\frac{\partial^2}{\partial\mu_1\,\partial\mu_2}[A_1A_2C_1C_2], \tag{75}$$

where

$$A_1 \equiv (A^*-\mu_1)^{i(\beta+m)}, \quad A_2 \equiv (A-\mu_2)^{-i(\beta-m)}, \quad C_1 \equiv (C^*-\mu_1)^{-i(\beta+m)}, \quad C_2 \equiv (C-\mu_2)^{i(\beta-m)},$$
$$A \equiv \tfrac{1}{4}\alpha(1+iv), \quad B \equiv (1+v^2), \quad C \equiv \tfrac{1}{4}\alpha(1+i/\gamma), \quad D \equiv (1+1/\gamma^2). \tag{76}$$

$C_{\mathfrak{K}ma}$ now has the value

$$C_{\mathfrak{K}m1} = \tfrac{1}{2}\pi^{-3/2}\mathfrak{K}^2e^{\pi\beta}|\Gamma[i(\beta+m)]||\Gamma[i(\beta-m)]|. \tag{77}$$

Performing the lengthy calculation in Eq. (75) and using the additional definitions

$$\theta_1 \equiv 1+\frac{2v}{\gamma}-\frac{1}{\gamma^2}, \quad \theta_2 \equiv -v+\frac{2}{\gamma}+\frac{v}{\gamma^2}, \quad \phi_1 \equiv 1+\frac{2v}{\gamma}-v^2, \quad \phi_2 \equiv \frac{1}{\gamma}-2v-\frac{v^2}{\gamma}, \tag{78}$$

$$q_{11}(\mathfrak{K}, m, k, 0) = \alpha(\tfrac{1}{4}\alpha)^{-3}\pi^{-3/2}e^{\pi\beta}|\Gamma[i(\beta+m)]||\Gamma[i(\beta-m)]|\,\frac{m^2-\beta^2}{B^{2-im}D^{2+im}}\exp\left(2\beta\tan^{-1}\frac{2P}{1+\kappa^2-P^2}\right)$$

$$\times\left[B(\theta_1-\beta\theta_2)+D(\phi_1-\beta\phi_2)-(D^2+B^2)-\beta BD^2\left(\frac{v}{B}-\frac{2}{\gamma D}\right)-\beta B^2D\left(\frac{2v}{B}-\frac{1}{\gamma D}\right)\right.$$

$$\left.+im(B\theta_1-D\phi_1+D^2-B^2)\right]. \tag{79}$$

We write the bracketed terms in this last equation as

$$\mathcal{R} + im\mathcal{I}. \tag{80}$$

Substituting Eq. (76) into Eq. (77) and taking the square of its absolute value, we get finally

$$|\epsilon_{211}(k)|^2 \equiv \int_{-\infty}^{\infty} |\epsilon_{211,\mathcal{R}m}(k)|^2\, dm$$
$$= \frac{64a_0}{B^4D^4Z} \exp\left(-\frac{4}{P}\tan^{-1}\frac{2P}{1+\kappa^2-P^2}\right)\left(\mathcal{R}^2\int_{-\infty}^{\infty}\frac{(\beta^2-m^2)\,dm}{(1-e^{-2\pi(\beta+m)})(1-e^{-2\pi(\beta-m)})}\right.$$
$$\left. + \mathcal{I}^2\int_{-\infty}^{\infty}\frac{m^2(\beta^2-m^2)\,dm}{(1-e^{-2\pi(\beta+m)})(1-e^{-2\pi(\beta-m)})}\right). \tag{81}$$

These integrals are evaluated in Appendix C, and have the values

$$\int_{-\infty}^{\infty}\frac{(\beta^2-m^2)\,dm}{(1-e^{-2\pi(\beta+m)})(1-e^{-2\pi(\beta-m)})} = \tfrac{1}{3}\beta(1+4\beta^2)(1-e^{-4\pi\beta})^{-1}, \tag{82}$$

$$\int_{-\infty}^{\infty}\frac{m^2(\beta^2-m^2)\,dm}{(1-e^{-2\pi(\beta+m)})(1-e^{-2\pi(\beta-m)})} = \tfrac{1}{15}\beta(1+5\beta^2+4\beta^4)(1-e^{-4\pi\beta})^{-1}. \tag{83}$$

As in the previous cases, going to atomic units Eq. (27) becomes

$$I \equiv I^{\text{exact}}_{2P^{(\pm1)}} = \frac{128}{15\times 27.212\,Z^2P^2}\left(\frac{E_2}{E_1}\right)B^{-4}D^{-4}(1-e^{-4\pi/P})^{-1}$$
$$\times\left[5\mathcal{R}^2\left(1+\frac{4}{P^2}\right)+\mathcal{I}^2\left(1+\frac{5}{P^2}+\frac{4}{P^4}\right)\right]\exp\left(-\frac{4}{P}\tan^{-1}\frac{2P}{1+\kappa^2-P^2}\right), \tag{84}$$

where

$$\mathcal{R} \equiv B\left(\theta_1-\frac{\theta_2}{P}\right)+D\left(\phi_1-\frac{\phi_2}{P}\right)-(D^2+B^2)-\frac{BD^2}{P}\left(\frac{v}{B}-\frac{2}{\gamma D}\right)-\frac{B^2D}{P}\left(\frac{2v}{B}-\frac{1}{\gamma D}\right),$$
$$\mathcal{I} \equiv B\theta_1 - D\phi_1 + D^2 - B^2, \tag{85}$$
$$\theta_1 \equiv 1+\frac{2v}{\gamma}-\frac{1}{\gamma^2}, \quad \theta_2 \equiv -v+\frac{2v}{\gamma}+\frac{v}{\gamma^2}, \quad \phi_1 \equiv 1+\frac{2v}{\gamma}-v^2, \quad \phi_2 \equiv \frac{1}{\gamma}-2v-\frac{v^2}{\gamma}.$$

The Compton profile is then given by

$$J^{\text{exact}}_{2P^{(\pm1)}} = (E_1/E_2)\,13.606\,\kappa Z\, I^{\text{exact}}_{2P^{(\pm1)}}. \tag{86}$$

IV. IMPULSE APPROXIMATION

The impulse hydrogenic (IH) approximation utilizes the hydrogenic momentum wave functions $\chi(\vec{p}_1)$ obtainable either from a Fourier transformation of the position wave functions $\psi(\vec{r})$ or directly as solution of the Schrödinger equation in a momentum representation. We will use the former method, thus

$$\chi(\vec{p}_1) = (2\pi\hbar)^{-3/2}\int e^{-i(\vec{p}_1\cdot\vec{r})/\hbar}\,\psi(\vec{r})\,d\vec{r}. \tag{87}$$

In terms of $I(p_1)$ where $I(p_1)\,dp_1$ is the probability that $\vec{p}_1$ has a magnitude between p_1 and p_1+dp_1 and therefore that

$$\int_0^{\infty} I(p_1)\,dp_1 = 1, \tag{88}$$

$J_{\text{imp}}(q)$ in Eq. (5) can be written in the form

$$J_{\text{imp}}(q) = \frac{1}{2}\int_{|q|}^{\infty}\frac{I(p_1)\,dp_1}{p_1}. \tag{89}$$

In terms of the momentum wave function $\chi(\vec{p}_1)$, $I(p_1)$ can be written as

$$I(p_1) = \int|\chi(\vec{p}_1)|^2 p_1^2\,d\omega, \tag{90}$$

where $d\omega$ is the solid angle subtended by $\vec{p}_1$. Duncanson and Coulson[15] showed that

$$\int_{-\infty}^{\infty} J_{\text{imp}}(q)\,dq = 1 \tag{91}$$

per electron within an independent-particle approximation. IH Compton profiles can therefore be evaluated for various electronic states from a knowledge of the corresponding bound-state wave functions. We proceed to perform this evaluation for K- and L-shell Compton profiles.

A. K-shell IH Compton profile

Starting with the spherically symmetric 1S bound-state hydrogenic wave function

$$\psi_{1S}(r) = (Z^3/\pi a_0^3)^{1/2} e^{-(r/a_0)Z} \tag{92}$$

in Eq. (87), we calculate $\chi(\vec{p}_1)$. Inserting this value into Eq. (90), we find that

$$I_{1S}(p_1) = \frac{32 p_1^2 Z^5}{\pi a_0^5 (p_1^2 + Z^2/a_0^2)^4} . \tag{93}$$

Inserting this expression into Eq. (89), we arrive at

$$J_{1S}^{\mathrm{imp}}(q) = \frac{8Z^5}{3\pi a_0^5 (q^2 + Z^2/a_0^2)^3} , \tag{94}$$

which on going over to atomic units ($q a_0 \to q$) finally becomes

$$J_{1S}^{\mathrm{imp}}(q) = \frac{8}{3\pi Z (1 + q^2/Z^2)^3} . \tag{95}$$

B. $2S$ IH Compton profile

Here we use the spherically symmetric 2S bound-state hydrogenic wave function

$$\psi_{2S}(r) = \frac{1}{4}\left(\frac{2Z^3}{\pi a_0^3}\right)^{1/2}\left(\frac{rZ}{2a_0} - 1\right) e^{-(r/2a_0)Z}, \tag{96}$$

and following the same procedure as for the K-shell, we get

$$J_{2S}^{\mathrm{imp}}(q) = \frac{64}{\pi Z}\left(\frac{1}{3(1 + 4q^2/Z^2)^3} - \frac{1}{(1 + 4q^2/Z^2)^4} + \frac{4}{5(1 + 4q^2/Z^2)^5}\right). \tag{97}$$

C. $2P$ IH Compton profile

There are three cases for the $2P$ electrons depending on the azimuthal quantum number m, namely $m = 0, \pm 1$. However, all three cases yield the same $I(p_1)$, i.e.,

$$I_{2P}(p_1) = \frac{4 \times 64^2}{3\pi} \frac{p_1^4}{(1 + 4p_1^2)^6} . \tag{98}$$

Finally substituting Eq. (97) into Eq. (89), we arrive at the desired result

$$J_{2P}^{\mathrm{imp}}(q) = \frac{64}{15\pi Z} \frac{1 + 20q^2/Z^2}{(1 + 4q^2/Z^2)^5} . \tag{99}$$

V. COMPARISON OF EH AND IH L-SHELL COMPTON PROFILES

A. Ratio of $2S$ IH and EH differential cross sections at the profile center

Following the K-shell derivation of the IH and EH differential cross sections at the profile center given previously,[29] and using

$$P^2 \equiv \left(\frac{n\mathcal{K}a_0}{Z}\right)^2 = 2\left(\frac{n^2 E}{27.212 Z^2} - \frac{1}{2}\right), \tag{100}$$

from conservation of energy in the Exact formulation, and also that

$$\kappa^2 \equiv \left(\frac{nka_0}{Z}\right)^2 = \frac{10^{-6} n^2}{0.511 Z^2 \times 27.212} (E_1^2 + E_2^2 - 2E_1 E_2 \cos 2\theta), \tag{101}$$

we define P^0 and κ^0 as the values of P and κ at the profile center. The left-hand sides of Eqs. (100) and (101) are in atomic units, while E_1 and E_2 are expressed in eV. Equation (3) may be written as

$$q = \frac{nE}{27.212 \kappa Z} - \frac{\kappa Z}{2n} , \tag{102}$$

and at the profile center

$$(\kappa^0)^2 = 1 + (P^0)^2. \tag{103}$$

The evaluation of the IH profile at the profile center is immediate; thus, setting $q = 0$ in Eq. (97), we find that

$$J_{2S}^{\mathrm{imp}}(0) = 128/15\pi Z. \tag{104}$$

The evaluation of the EH profile at the profile center requires that we expand the terms in the exact profile for P^0, κ^0 greater than 1. Thus Eq. (66) becomes

$$J_{2S}^{\mathrm{exact}}(\kappa^0) \approx \frac{128}{15\pi Z}\left(1 - \frac{1.205}{(\kappa^0)^2}\right)\left(1 + \frac{1}{2(\kappa^0)^2}\right) \approx \frac{128}{15\pi Z}\left(1 - \frac{0.705}{(\kappa^0)^2}\right). \tag{105}$$

Finally, the desired ratio is given by

$$\left(\frac{J_{2S}^{\mathrm{imp}}}{J_{2S}^{\mathrm{exact}}}\right)_{q=0} \approx \frac{128/15\pi Z}{(128/15\pi Z)(1 - 0.705/(\kappa^0)^2)} \approx \left(1 + \frac{0.705}{(\kappa^0)^2}\right). \tag{106}$$

Making use of the definition of κ [Eq. (101)], Eq. (106) can be written as

$$\left(\frac{J_{2S}^{\mathrm{imp}}}{J_{2S}^{\mathrm{exact}}}\right)_{q=0} \approx \left(1 + \frac{0.176}{(k^0 a_0/Z_{2S}^*)^2}\right), \tag{107}$$

where k^0 is evaluated at $q = 0$ and Z_{2S}^* is related to the 2S binding energy. Previously, for the 1S ratio[29]

$$\left(\frac{J_{1S}^{\mathrm{imp}}}{J_{1S}^{\mathrm{exact}}}\right)_{q=0} \approx \left(1 + \frac{0.145}{(k^0 a_0/Z_{1S}^*)^2}\right), \tag{108}$$

with Z_{1S}^* related to the 1S binding energy, Z_{1S}^* is always greater than Z_{2S}^*. For the cases we have

looked at IH is a better approximation to EH at the profile center for the 2S case than for the corresponding 1S case. For example, for the case of boron we find

$$\left(\frac{J_{2S}^{\text{imp}}}{J_{2S}^{\text{exact}}}\right)_{q=0} \approx \left(1+\frac{0.696}{(k^0a_0)^2}\right),$$
$$\left(\frac{J_{1S}^{\text{imp}}}{J_{1S}^{\text{exact}}}\right)_{q=0} \approx \left(1+\frac{2.000}{(k^0a_0)^2}\right). \tag{109}$$

B. 2S Compton profiles

Unlike the 1S curves, which exhibit a single maximum in both the EH and IH profiles, the 2S curves have structure, with the EH having a secondary maximum (SM) and the IH having a plateau.[30] Figures 1–8 portray the EH and IH differential cross sections for a 20 000-eV incident photon scattered by materials having either a Z of 2 or 5 and for selected scattering angles. The IH curves are monotonic and symmetric about $q=0$, the profile center. The onset of the SM in the EH is seen to coincide in all cases with the plateau in the IH. This plateau will be shown to occur around $-q=Z/2$ and is related to a node in the momentum wave function. As in the 1S case (Ref. 29), the two curves are seen to cross near the profile center, and the ratio of IH to EH at $q=0$ is less than for K-shell elec-

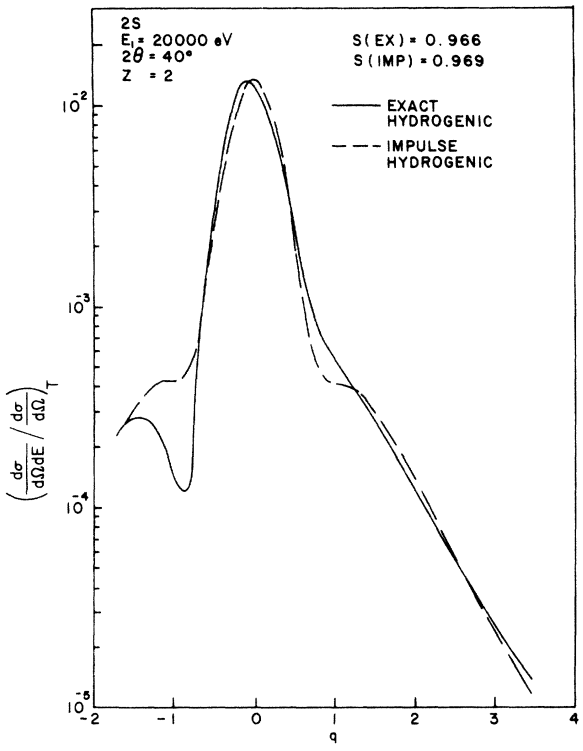

FIG. 1. Compton scattering from a 2S electron.

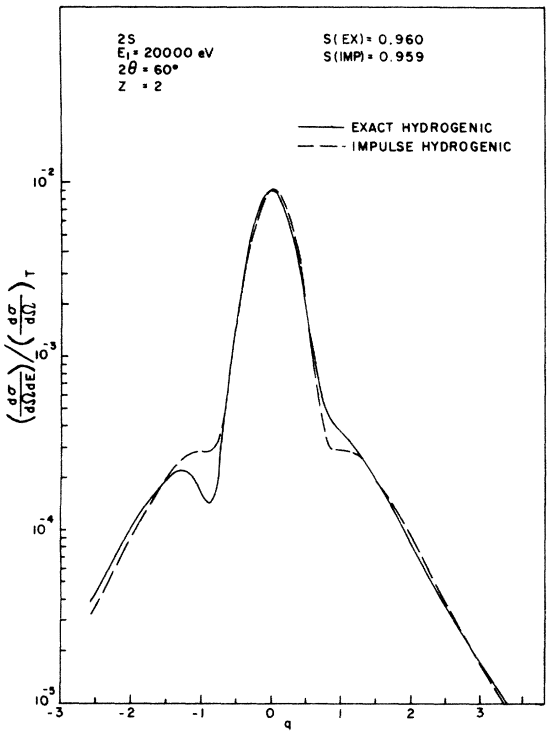

FIG. 2. Compton scattering from a 2S electron.

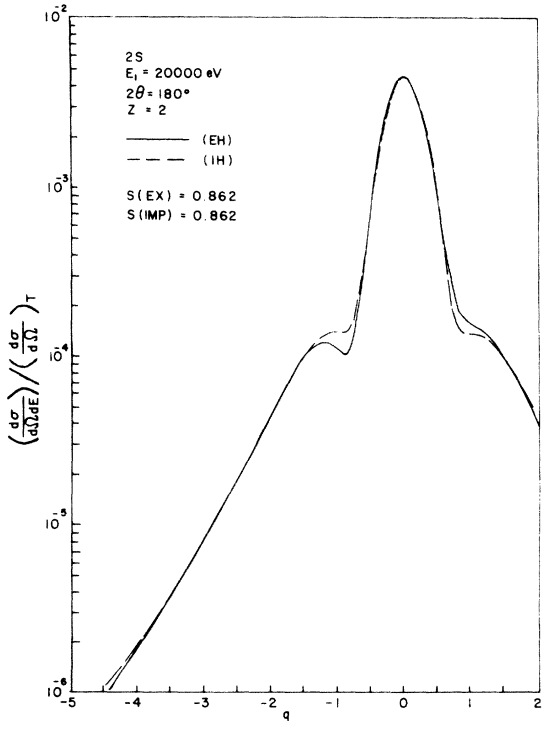

FIG. 3. Compton scattering from a 2S electron.

trons for the typical cases we have outlined before, indicating that the IH is improved over the 1S case.

As noted for the K-shell results, as the scattering angle is decreased (and also therefore the momentum transfer), the left-hand side of the profile cuts off at larger values of q. For $Z=2$ and $2\theta=60°$, q cutoff is at -2.6, while for $2\theta=40°$, q cutoff is at 1.7, as can be seen by examining Figs. 1 and 2. When $Z=5$, $2\theta=60°$ (Fig. 5) the curve cuts off so soon that the SM is not reached. This occurs because for $Z=5$ the onset of the SM begins at a $-|q|$ of about 2.5. When the incident photon energy is decreased for fixed scattering angles and binding energy, the profile width decreases and one can obtain less than one half a profile. In the region about the secondary maximum the EH calculation naturally gives a large correction to the IH calculation. For example, for $Z=5$, $2\theta=90°$ (Fig. 6) the SM occurs slightly above the binding energy, and the difference between the IH and the EH at $-q=2.35$ is 400%! It is in the region near the binding energy that the IH is least correct, the rule of thumb being that the IH is a reasonable approximation when the energy transferred to the electron is at least twice the binding energy. This case is further complicated by the fact that near ionization threshold the independent-particle model calculation

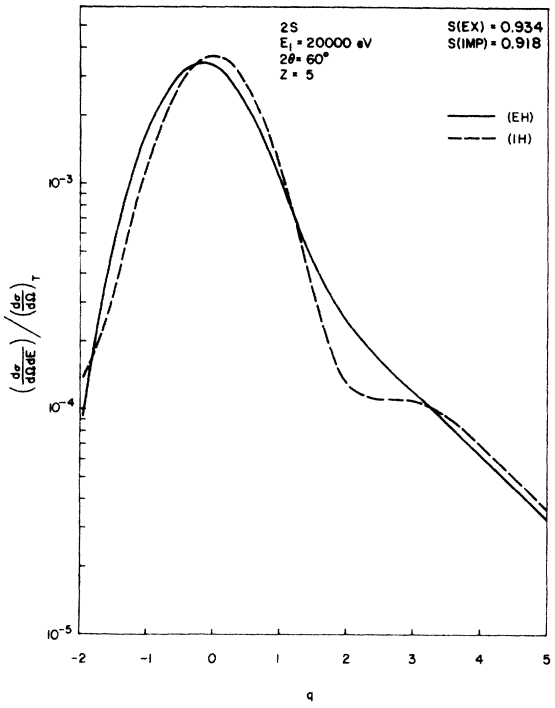

FIG. 5. Compton scattering from a 2S electron.

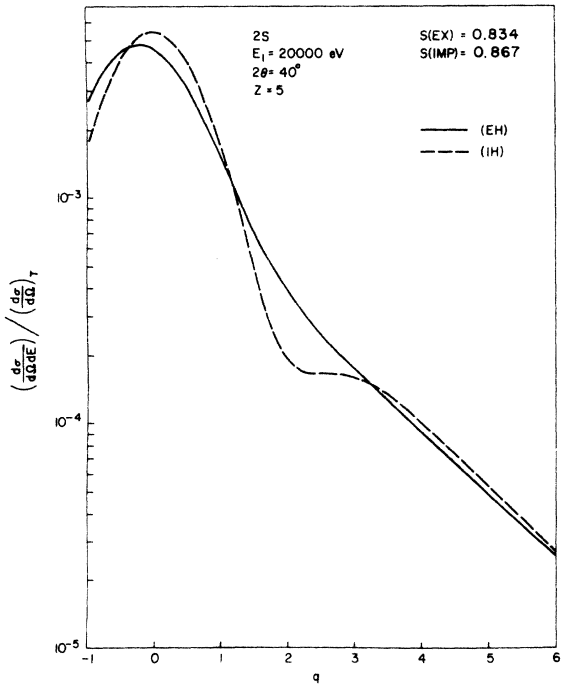

FIG. 4. Compton scattering from a 2S electron.

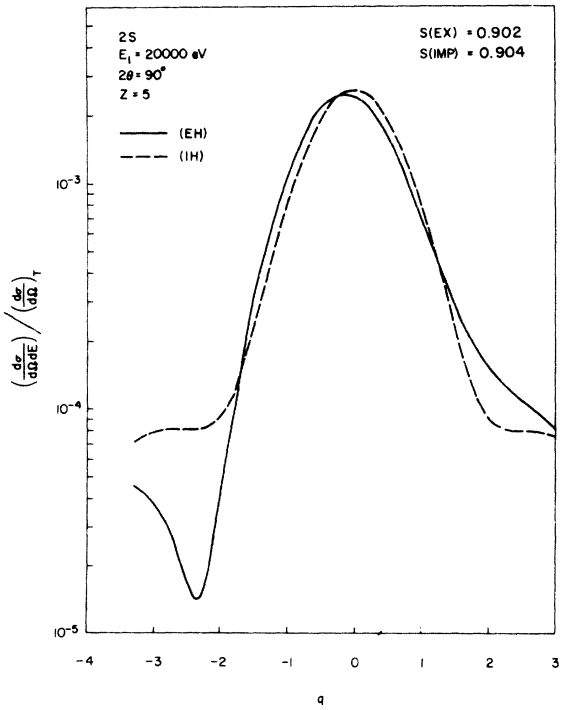

FIG. 6. Compton scattering from a 2S electron.

of the ionization process is not a very accurate description. Looking at a typical SM we see that in order for it to be observed, an energy resolution exceeding a Δq of $\frac{1}{2}$ a.u. is called for. In addition the secondary maximum structure may only be seen if the intensity of the source is increased to show cross-section profiles that are more than one order of magnitude down from the center of the profile. As q at cutoff increases in magnitude, the impulse approximation gets progressively worse, and cannot be used to determine profile structure.

C. $2P$ Compton profiles

The IA does not distinguish between the $2P^{(\pm 1)}$ and $2P^{(0)}$ states, but the EH evaluation results in two markedly distinct profiles. Figures 9–12 show the differential cross sections for an incident 20 000-eV photon and for $Z=2$ and $Z=5$ with scattering angles of 30° and 180°. Like the $2S$ state, the $2P^{(0)}$ profile exhibits structure; however, unlike the relatively small peak in the $2S$, the two maxima in the $2P^{(0)}$ profiles are of the same order of magnitude. The same cutoff conditions apply for the $2P$ profiles, as we demonstrated in the $1S$ and $2S$ cases. We see from Fig. 11 that the low-scattering-angle higher-Z material at the cutoff results in slightly more than one half a profile with the absence of a SM. The IH profiles in Figs. 9–12 seem to average the

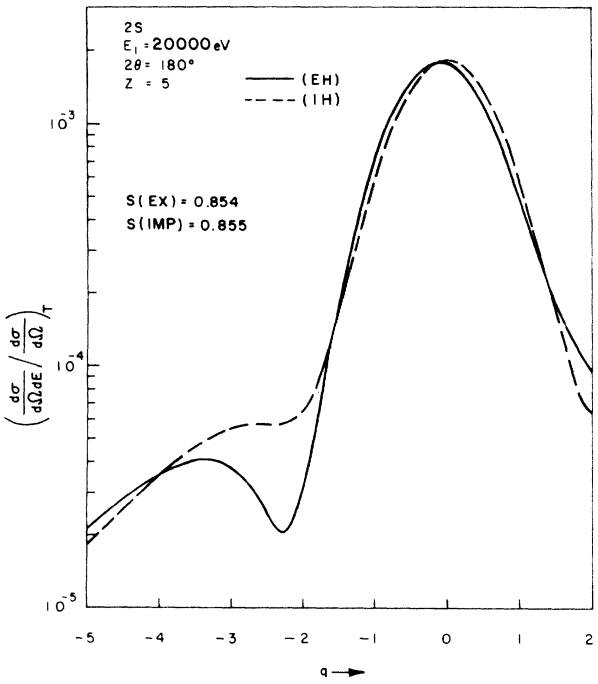

FIG. 8. Compton scattering from a $2S$ electron.

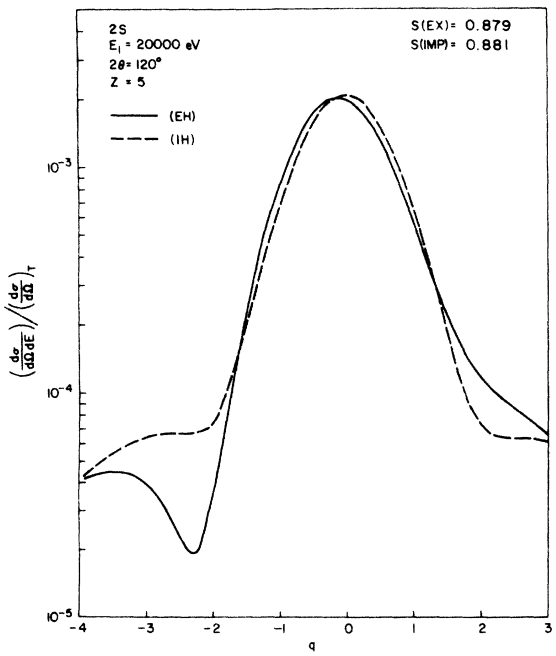

FIG. 7. Compton scattering from a $2S$ electron.

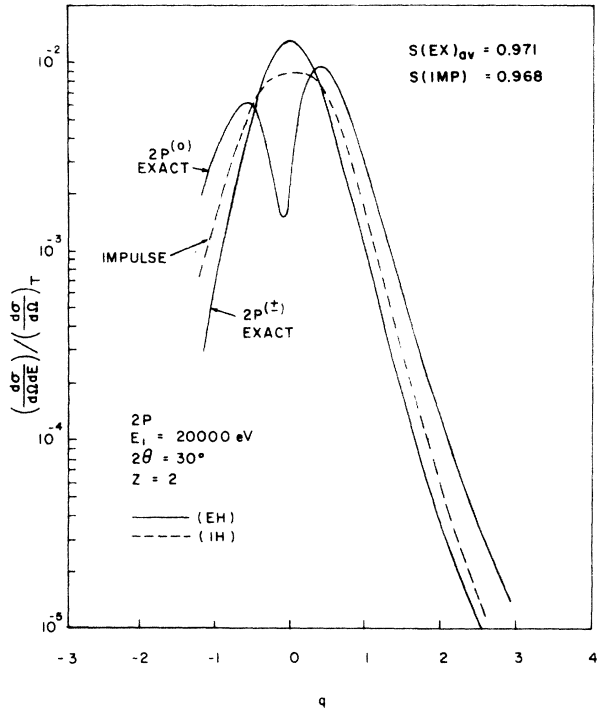

FIG. 9. Compton scattering from a $2P$ electron.

$2P^{(\pm1)}$ and $2P^{(0)}$ results. Since there are two electrons in the $2P^{(\pm1)}$ state and one electron in the $2P^{(0)}$, we will always use an averaged EH $2P$ value. Figure 13 shows a comparison of the IH and averaged EH $2P$ profiles for $E_1 = 20\,000$ eV, $Z = 5$ and $2\theta = 180°$. The EH $2P$ (unless otherwise specified when we refer to the EH $2P$ results, we will mean the averaged $2P^{(0)}$, $2P^{(\pm1)}$ values) is seen to peak to the right of the profile center. Again the tendency for the IH and EH profiles to cross, as seen in the $1S$ and $2S$ cases, is also observed for the $2P$ case. The relative sharp peak in the single maximum $2P^{(\pm1)}$ when averaged with the $2P^{(0)}$ profile appears to result in a very flat region at $q = 0$. This flatness is observed in both the IH and in Weiss's impulse Hartree-Fock (IHF) Clementi free-atom profiles.

VI. SECONDARY MAXIMUM ANALYSIS

A. Relation to momentum wave function

We now want to examine the additional feature contained in the EH and IH $2S$ and $2P^{(0)}$ Compton profiles. Starting with Eq. (89) and integrating over the directions of the initial electron momentum, we obtain

$$J_{\rm imp}(q) = 2\pi \int_{|q|}^{\infty} |\chi(\vec{p}_1)|^2 p_1\, dp_1. \tag{110}$$

One can invert Eq. (110) to obtain $|\chi(\vec{p}_1)|^2$; thus

$$|\chi(\vec{p}_1)|^2 = \left| \frac{1}{2\pi q} \frac{dJ_{\rm imp}}{dq} \right|. \tag{111}$$

Two properties of $J_{\rm imp}(q)$ are discernible from a study of Eq. (111). The first is that $J_{\rm imp}(q)$ is a symmetric function in q; the second is that $J_{\rm imp}(q)$ is a monotonic decreasing function with increasing $|q|$. From Eq. (111) we note that when $|\chi(\vec{p}_1)|^2$ is zero, $dJ_{\rm imp}/dq$ is also zero for finite $|q|$. Therefore, combined with the second property, a zero in the momentum wave function $\chi(\vec{p}_1)$ will produce a flat region in the $J_{\rm imp}(q)$ profile. We will examine the $2S$ and $2P$ IH profile to determine the values of q that correspond to a flat region in $J_{\rm imp}(q)$.

For the $2S$ IH profile, $J_{2S}^{\rm imp}(q)$ is given by Eq. (97)

$$J_{2S}^{\rm imp}(q) = \frac{64}{\pi Z}\left(\frac{1}{3(1+4q^2/Z^2)^3} - \frac{1}{(1+4q^2/Z^2)^4} + \frac{4}{5(1+4q^2/Z^2)^5} \right).$$

Taking the derivative with respect to q, we obtain

$$\frac{dJ_{2S}^{\rm imp}(q)}{dq} = \frac{8\times 64}{\pi Z^3} q\left(\frac{-1}{(1+4q^2/Z^2)^4} + \frac{4}{(1+4q^2/Z^2)^5} - \frac{4}{(1+4q^2/Z^2)^6} \right). \tag{112}$$

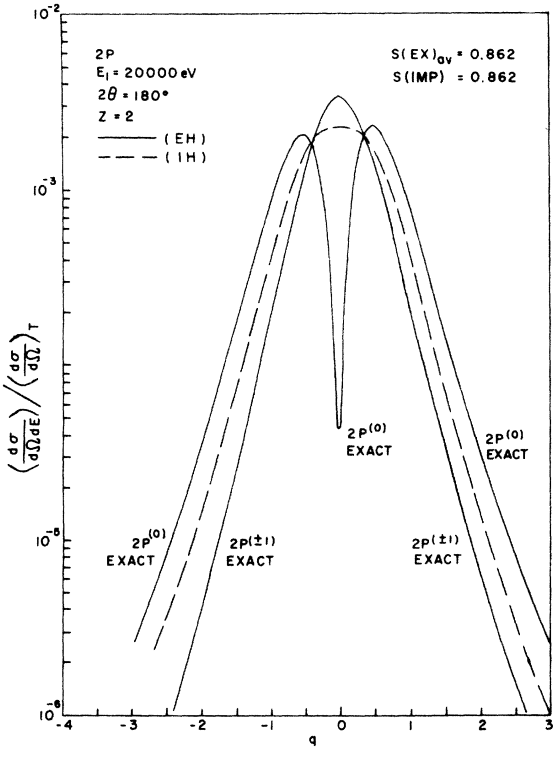

FIG. 10. Compton scattering from a $2P$ electron.

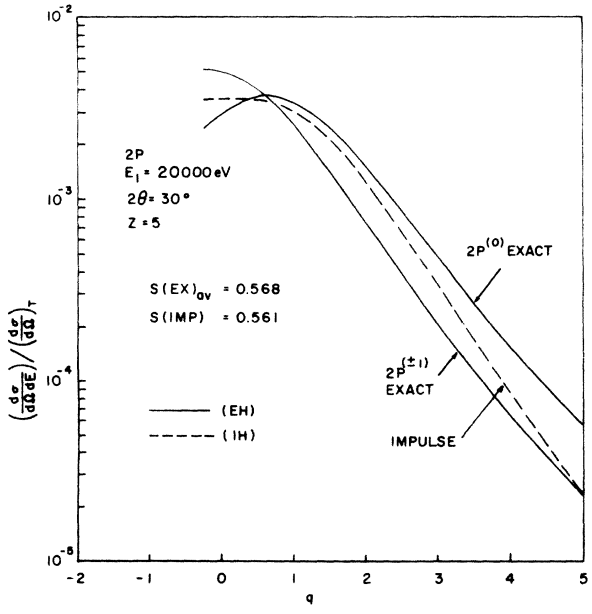

FIG. 11. Compton scattering from a $2P$ electron.

Setting Eq. (111) equal to zero and solving for q, i.e.,

$$\frac{1}{q}\frac{dJ_{2S}^{\mathrm{imp}}(q)}{dq}=0,$$

we obtain

$$4q^2/Z^2=1. \tag{113}$$

Thus the $J_{2S}^{\mathrm{imp}}(q)$ profile will have a flat region at $q=\pm Z/2$. This corresponds to the value of momentum where the 2S momentum wave function has a node.

Following the same procedure for $J_{2P}^{\mathrm{imp}}(q)$, and using Eq. (99), namely,

$$J_{2P}^{\mathrm{imp}}(q)=\frac{64}{15\pi Z}\frac{1+20q^2/Z^2}{(1+4q^2/Z^2)^5},$$

we calculate that the plateau will occur at $q=0$.

B. Nodal behavior in momentum and spatial wave functions

The functional relationship between nodes in momentum and configuration space may be studied via the Fourier transformation. Thus in atomic units

$$\chi(\vec{p}_1)=\frac{1}{(2\pi)^{3/2}}\int_{-\infty}^{\infty}\psi(\vec{r})\,e^{-i\vec{p}_1\cdot\vec{r}}\,d\vec{r}, \tag{114}$$

which for spherically symmetric states becomes

$$\chi(p_1)=\frac{2}{(2\pi)^{1/2}p_1}\int_0^{\infty}\sin(p_1r)\psi(r)\,dr. \tag{115}$$

To be physically meaningful, we demand that $\psi(r)$ be quadratically integrable, and, since we are interested in bound-state wave functions, use $\psi(r)$ in the form

$$\psi(r)=f(r)\,e^{-ar},\quad a>0. \tag{116}$$

We now take $f(r)$ to be a polynomial in r, thus providing flexibility in the number of zeros in $\psi(r)$, and at the same time ensuring convergence of the Fourier integral. Equation (115) therefore assumes the form for this $\psi(r)$

$$\chi(\vec{p}_1)=\int_0^{\infty}\sum_{m=0}^{s}\left[2b_m/(2\pi)^{1/2}p_1\right]\times(r^{m+1}\sin(p_1r)\,e^{-ar}\,dr), \tag{117}$$

having written $f(r)$ as

$$f(r)=\sum_{m=0}^{s}b_m r^m, \tag{118}$$

where the b_m are constants. Now the summation over m in Eq. (117) commutes with the integral sign, and making use of the integral identity

$$\int_0^{\infty}r^n e^{-ar}\sin(p_1r)\,dr=\frac{in!\left[(a-ip_1)^{n+1}-(a+ip_1)^{n+1}\right]}{2(a^2+p_1^2)^{n+1}}, \tag{119}$$

where $a>0$, Eq. (117) becomes

$$\chi(p_1)=\sum_{m=0}^{s}\frac{2b_m(m+1)!}{(2\pi)^{1/2}}\frac{1}{p_1}\frac{\sin[(m+2)\varphi]}{(a^2+p_1^2)^{1+m/2}}, \tag{120}$$

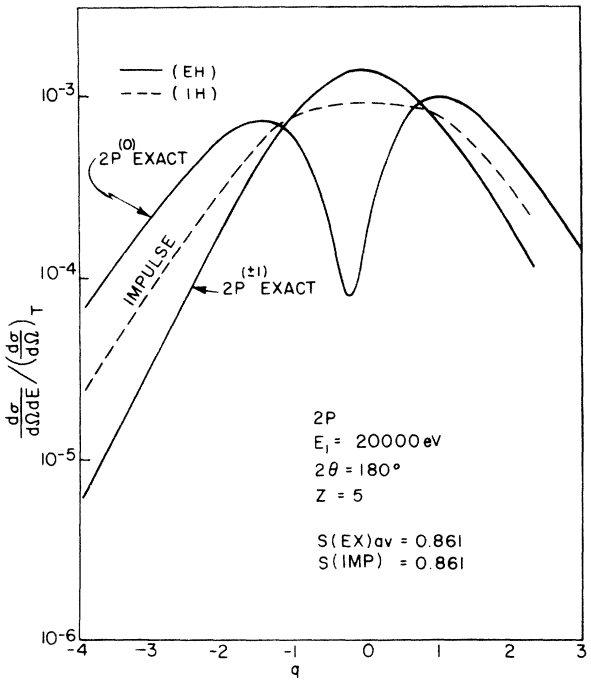

FIG. 12. Compton scattering from a 2P electron.

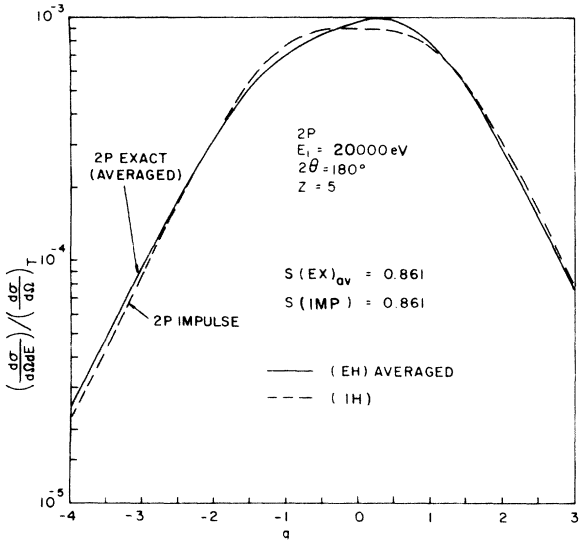

FIG. 13. Averaged exact vs impulse Compton scattering from a 2P electron.

where

$$\varphi \equiv \tan^{-1}(p_1/a). \tag{121}$$

$\chi(p_1)$ is a polynomial of order s in p_1^2. Thus we have a one-to-one correspondence of the nodes in the configuration wave function to the nodes in the momentum wave function. For bound systems that have eigenvalues that can be ordered, corresponding to orthogonal eigenfunctions with uniformly increasing number of nodes, the complimentary momentum space, preserving this eigenfunction orthogonality, will therefore exhibit the same nodal behavior.

One can readily calculate the product of the widths (distance from the origin) of the nodes in configuration space and momentum space for hydrogenic 2S bound-state wave functions. We find $\Delta p = Z/2$ and $\Delta r = 2/Z$ in a.u., which gives the product $\Delta r \Delta p = 1$. For higher-lying hydrogenic states n with one node ($l = n - 1$), one observes $\Delta r \Delta p = n - 1$. These results follow the expected pattern that as Z increases the spatial wave function (electron density) is pulled in and the momentum density is pushed out. This effect is exhibited in the Compton profile as a zero-slope region in the IH profile.

Our hydrogenic calculations show that the EH profile has a secondary maximum at the same approximate value of $-|q|$ at which the IH exhibits its plateau. For the 2S EH profile, the secondary maximum is down by more than an order of magnitude from the primary central maximum. From the foregoing analysis the secondary maximum appears to be related to the structure of the electron density in the original wave function. Since Hartree-Fock wave functions exhibit the same type of nodal structure as the hydrogenic wave functions, we expect secondary maxima to occur when Hartree-Fock calculations are performed.

When the change in the photon energy E is small, the time spent in probing the electronic structure is large (since $E\Delta t \sim \hbar$ from the uncertainty principle), and therefore the exact Compton profile would show greater structure than when the change in photon energy is large. This indeed appears to be the case, as the secondary maximum is only found on the low-momentum transfer $-|q|$ side of the profile. This too is the side of the profile where qualitatively we would expect a larger deviation of the EH from the IH profile, since the impulse approximation explicitly assumes small interaction times and large values of E.

Assuming that strong-intensity x-ray sources become available to accurately experimentally probe this region of the profile, we would expect the SM phenomena to be most easily demonstrated for small angle scattering from lithium and beryllium in its gaseous form. We specify small angles because if the 1S state was also excited, the 1S profile would tend to dominate at q values corresponding to the SM and wash out the effect. We note that Cohen and Alexandropoulos[31] have performed small angle scattering from lithium in crystal form and have observed resonances in their valence electron profile. These resonances are usually associated with either Raman transitions or plasmon excitations. In certain cases the position of the resonance agrees with our calculated values but the intensity observed by them is much larger than we would calculate. Their SM intensity appears almost as large as the intensity at the profile center. No normalized values of their results are given, however. In addition, in the solid, orbital angular momentum is no longer a good quantum number, although one would expect the 2S state to play an important role in any atomic-orbital expansion of the Bloch wave describing the valence electron. Thus one would expect our atomic results to be somewhat washed out, rather than enhanced in the solid. We feel that our SM have not yet been experimentally observed, but may well prove an important test on the accuracy of atomic wave functions because they are intimately related to the nodal structure in the atomic wave functions.

VII. INCOHERENT SCATTERING FACTORS

A. Waller-Hartree calculation

Starting with Eq. (15) we calculate the coherent-scattering factor F, where

$$F(k) = 4\pi \int_0^\infty \rho(r)[(\sin kr)/kr]\, r^2\, dr, \tag{122}$$

and $\rho(r)$ denotes the electron density $|\psi(r)|^2$.

1S state

Here

$$\rho(r) = (Z^3/\pi a_0^3)\, e^{-(2r/a_0)Z},$$

and Eq. (122) becomes

$$F(k) = (1 + k^2/4Z^2)^{-2}. \tag{123}$$

Since $k = W/0.1504$, Eq. (123) becomes

$$F_{1S}(W) = \left[1 + \left(\frac{W}{0.1504}\right)^2 \frac{1}{4Z^2}\right]^{-2}. \tag{124}$$

2S state

Here we use the $\rho(r)$ corresponding to the 2S case and Eq. (122) becomes

$$F(k) = \left(\frac{Z}{2a_0}\right)^3 \int_0^\infty \frac{r}{k}\left(2 - \frac{rZ}{a_0}\right)^2 \times e^{-(r/a_0)Z} \sin(kr)\, dr. \tag{125}$$

This integral can be evaluated by making use of the integral identity (119), and since $k = W/0.1504$, we arrive at

$$F_{2S}(W) = [1 + (W/0.1504Z)^2]^{-4} \times [1 - 3(W/0.1504Z)^2 + 2(W/0.1504Z)^4]. \quad (126)$$

$2P^{(0)}$ state

Equation (15) when evaluated for this case becomes

$$F_{2P^{(0)}}(W) = [1 + (W/0.1504Z)^2]^{-4} \times [1 - 5(W/0.1504Z)^2]. \quad (127)$$

$2P^{(\pm 1)}$ state

Here the evaluation of Eq. (15) leads to

$$F_{2P^{(\pm 1)}}(W) = [1 + (W/0.1504Z^2]^{-3}. \quad (128)$$

The Waller-Hartree incoherent-scattering factors S(WH) for the 1S and 2S electron states can now be evaluated by substituting Eq. (17) into Eq. (16), yielding

$$S(\mathrm{WH}) = (E_2^0/E_1)^2(1 - |F|^2), \quad (129)$$

and then replacing F in the equation by the appropriate F from Eqs. (124) and (126)–(128). We note that Bonham[32] has considered corrections to the Waller-Hartree result.

B. Comparison of EH, IH, and Waller-Hartree incoherent-scattering factors

Incoherent-scattering factors are calculated, for incident photon energies of 5000 to 60 000 eV ($Z = 5$) and scattering angles of 30°–180°. These factors are calculated for the 2S, $2P^{(0)}$, and $2P^{(\pm 1)}$ electrons. We call S(EX) and S(IMP) the values for the incoherent-scattering factors calculated using Eq. (19) in the EH and IH formulations, respectively.

The 2S scattering factors for $Z = 5$, variable incident photon energy, and variable angles are given in Tables I–IV, for S(EX) and S(IMP). One sees that for energies E_1 greater than 30 000 eV, S(IMP) is a good approximation to S(EX), the relative difference being less than 0.2%. As the scattering angle increases, the relative difference for fixed $E_1 > 5000$ eV improves as expected, owing to the greater momentum transfer. However, when E_1 is fixed at 5000 eV we observe that S(IMP) at first gets worse and then improves with increasing angle. The reason is that the Compton-profile cutoff varies with angle, and since the EH and IH curves cross at a number of points, the values of S obtained by integrating the Compton profiles over energy vary in a nonuniform fashion. Thus when one might expect S(IMP) to get worse, it can actually improve. A glance at Table V reveals this property, observed at fixed $E_1 = 17\,374$ eV, $2\theta = 170°$ and for varying Z^* chosen by matching the experimental binding energies with a hydrogenic model. As Z^* increases, S(IMP)/S(EX) tends to meander about 1, finally becoming 1.12 for Cr. Thus, even at this relatively large binding, the impulse approximation differs from the exact factor by only 12%. Throughout the lower binding energies the ratio S(IMP)/S(EX) is never far from 1. However, the

TABLE I. Compton scattering—variable energy.

$Z = 5$; $2\theta = 40°$			
E_1(eV)	S(IMP)	S(EX)	$\frac{S(\mathrm{IMP}) - S(\mathrm{EX})}{S(\mathrm{EX})}$ (%)
5000	0.029	0.030	−3.3
10 000	0.151	0.176	−14.2
15 000	0.613	0.578	+6.0
20 000	0.867	0.834	+3.96
30 000	0.931	0.945	−1.48
40 000	0.940	0.939	+0.106
50 000	0.944	0.942	+0.21
60 000	0.943	0.942	+0.106

TABLE II. 2S Compton scattering—variable energy.

$Z = 5$; $2\theta = 60°$			
E_1(eV)	S(IMP)	S(EX)	$\frac{S(\mathrm{IMP}) - S(\mathrm{EX})}{S(\mathrm{EX})}$ (%)
5000	0.052	0.073	−28.8
10 000	0.573	0.492	+16.5
15 000	0.890	0.994	+0.68
20 000	0.918	0.934	−1.71
30 000	0.925	0.923	+0.217
40 000	0.921	0.920	+0.109
50 000	0.910	0.910	...
60 000	0.896	0.896	...

TABLE III. 2S Compton scattering—variable energy.

$Z = 5$; $2\theta = 90°$			
E_1(eV)	S(IMP)	S(EX)	$\frac{S(\mathrm{IMP}) - S(\mathrm{EX})}{S(\mathrm{EX})}$ (%)
5000	0.168	0.186	−9.68
10 000	0.861	0.838	+2.74
15 000	0.903	0.915	−1.31
20 000	0.904	0.902	+0.22
30 000	0.889	0.888	...
40 000	0.863	0.863	...
50 000	0.835	0.836	...
60 000	0.809	0.809	...

Waller-Hartree $S(\mathrm{WH})/S(\mathrm{EX})$ ratio, although close to 1 over most of the range, is seen to become progressively worse for large binding. Thus for Cr the Waller-Hartree incoherent scattering factor differs from the exact by over 50%. That the Waller-Hartree results give poorer agreement with exact ones as the binding increases is, for the most part, caused by the fact that, when there is only a half-profile or less, it is quite clear[29] that using $(E_2^0/E_1)^2$ as the appropriate average outside the sum in Eq. (12) will give a large overestimate to the scattering. Any E_2 in the partial profile is less than E_2^0. Therefore, using E_2^0 as the average value must give a too-large value of $S(\mathrm{WH})$.

Thus for 2S scattering, the IA is a good representation for Z^* up to vanadium ($Z^*=13.58$), and even the Waller-Hartree factors are closer than for the 1S case (see Ref. 29). We therefore see the importance of the binding energy on the validity of the impulse and Waller-Hartree approximations.

It follows that S, given by Eq. (17) in the incoherent-scattering-factor approximation [Eq. (14)], is only a function of $W=\sin\theta/\lambda_1$. Now S [Eq. (17)] $=(E_1/E_2^0)^2 S(\mathrm{WH})$. Thus, to test this against the exact results, we have computed $(E_1/E_2^0)^2 S(\mathrm{EX})$. Tables VII–X show various E_1 for $Z=5$ and $\sin\theta/\lambda_1=0.2$; 0.4; 0.8; and 1.2 Å^{-1}. $(E_1/E_2^0)^2 S(\mathrm{WH})$ is nearly constant for all of these cases, varying from 0.987 for 0.4 Å^{-1} to 0.998 for 1.2 Å^{-1}. $(E_1/E_2^0)^2 S(\mathrm{EX})$ is also fairly constant, being 0.971 for 0.8 Å^{-1} and 0.977 for 1.2 Å^{-1}. However, for $\sin\theta/\lambda_1=0.4$ Å^{-1}, $(E_1/E_2^0)^2 S(\mathrm{EX})=0.49$, while $(E_1/E_2^0)^2 S(\mathrm{WH})=0.99$, a difference of 100%; at $\sin\theta/\lambda_1=0.2$, the difference is over 700%. Thus Waller-Hartree 2S calculations are more accurate than for the 1S case, but are still quite poor for small momentum transfers.

The 2P incoherent-scattering factors for the EH and Waller-Hartree calculations both yield different values for $2P^{(0)}$ and $2P^{(\pm1)}$. This distinction is not present in the IH or IHF results. We will therefore use the statistically weighted average $S(\cdots)_{\mathrm{av}}$ given by

$$S(\cdots)_{\mathrm{av}} \equiv \tfrac{1}{3}\left[S(\cdots)_{2P^{(0)}} + 2S(\cdots)_{2P^{(\pm1)}}\right], \quad (130)$$

where we insert either EH or WH in the parentheses to denote the particular calculation, and where $S(\cdots)_{2P^{(0)}}$ and $S(\cdots)_{2P^{(\pm1)}}$ are the $2P^{(0)}$ and $2P^{(\pm1)}$ incoherent scattering factors, respectively.

Table VI lists the 2P incoherent scattering factors for EH, IH, and WH with $E_1=17\,374$ eV, $2\theta=170°$ and variable binding. A comparison with Table V for the 2S incoherent-scattering factors reveals that with increasing binding the 2P state $S(\mathrm{IMP})$ and $S(\mathrm{WH})_{\mathrm{av}}$ values are closer to $S(\mathrm{EX})_{\mathrm{av}}$ than are the corresponding 2S state values. Tables XI–XIII show $S(\mathrm{IMP})$ and $S(\mathrm{EX})_{\mathrm{av}}$ for E_1 from 5000 to 60 000 eV; $2\theta=30°$, 90°, and 180°; and $Z=5$. As the scattering angle increases, the IH gets better over a larger range in E_1. Thus for $2\theta=30°$, $S(\mathrm{IMP})$ is close to $S(\mathrm{EX})_{\mathrm{av}}$ for $E_1 \geq 40\,000$ eV; while for $2\theta=180°$, $S(\mathrm{IMP}) \sim S(\mathrm{EX})_{\mathrm{av}}$ for $E_1 \geq 20\,000$ eV. In general, the $S(\mathrm{IMP})$ for the 2P state is closer to $S(\mathrm{EX})_{\mathrm{av}}$ than $S(\mathrm{IMP})$ is to $S(\mathrm{EX})$ for the 2S case. Figure 14 summarizes these results, and we see that as E_1 increases, all of the incoherent scattering factors (1S, 2S and 2P factors) approach $(E_2^0/E_1)^2$.

TABLE IV. 2S Compton scattering—variable energy.

$Z=5$; $2\theta=180°$			
E_1(eV)	$S(\mathrm{IMP})$	$S(\mathrm{EX})$	$\frac{S(\mathrm{IMP})-S(\mathrm{EX})}{S(\mathrm{EX})}$ (%)
5000	0.553	0.473	+16.9
10 000	0.882	0.898	−1.78
15 000	0.874	0.871	+0.34
20 000	0.855	0.854	···
30 000	0.804	0.804	···
40 000	0.754	0.754	···
50 000	0.708	0.708	···
60 000	0.667	0.667	···

VIII. CONCLUSIONS

Analytic results for "exact" hydrogenic (EH) L-shell Compton profiles have been obtained. Impulse approximation hydrogenic (IH) profiles were also calculated and comparisons with the EH profiles show that the two profiles lie very close

TABLE V. 2S Compton scattering—variable binding.

$E_1=17\,374$ eV; $2\theta=170°$				
	Z^*	$S(\mathrm{EX})$	$S(\mathrm{IMP})/S(\mathrm{EX})$	$S(\mathrm{WH})/S(\mathrm{EX})$
Li	1.25	0.879	0.999	0.998
Be	1.57	0.879	0.999	0.998
B	1.99	0.879	0.999	0.998
C	2.38	0.879	0.999	0.998
O	2.64	0.878	0.999	0.998
Ne	3.64	0.875	1.00	1.00
Na	4.32	0.870	1.00	1.00
Mg	5.13	0.863	1.00	1.01
Al	5.88	0.856	1.00	1.02
Si	6.61	0.851	0.999	1.02
Ar	9.70	0.843	0.980	1.04
V	13.58	0.663	1.08	1.32
Cr	14.85	0.568	1.12	1.54

TABLE VI. $2P$ Compton scattering—variable binding.

$E_1 = 17374$ eV; $2\theta = 170°$

	Z^*	$S(EX)$		$S(WH)/S(EX)$		$S(EX)_{av}$	$\frac{S(IMP)}{S(EX)_{av}}$	$\frac{S(WH)_{av}}{S(EX)_{av}}$
		$2P^{(0)}$	$2P^{(\pm 1)}$	$2P^{(0)}$	$2P^{(\pm 1)}$			
Li	1.25	0.879	0.879	0.998	0.998	0.879	1.00	0.998
Be	1.57	0.879	0.879	0.998	0.998	0.879	1.00	0.998
B	1.99	0.879	0.879	0.998	0.998	0.879	1.00	0.998
C	2.38	0.879	0.879	0.998	0.998	0.879	1.00	0.998
O	2.64	0.879	0.879	0.998	0.998	0.879	1.00	0.998
Ne	3.64	0.878	0.879	0.999	0.998	0.879	1.00	0.998
Na	4.32	0.875	0.879	1.00	0.998	0.878	1.00	0.999
Mg	5.13	0.865	0.879	1.01	0.998	0.875	1.00	1.00
Al	5.88	0.849	0.878	1.03	0.999	0.869	1.00	1.01
Si	6.61	0.826	0.876	1.05	1.00	0.860	1.00	1.01
Ar	9.70	0.685	0.831	1.19	1.03	0.782	0.994	1.08
V	13.58	0.572	0.640	1.41	1.23	0.618	0.959	1.28
Cr	14.85	0.541	0.559	1.52	1.35	0.553	0.966	1.40

to one another for weak-binding and high-incident photon energies. The ratio of the EH to IH 2S profile intensity at the unperturbed profile center is found, and it is observed that corrections to the IH profile are of the order of [Z/momentum transfer)]^2, where Z is the effective nuclear charge, at the profile center. This is similar to the analogous result for K-shell scattering obtained previously. As in the 1S case, the IH 2S profile always lies above the EH 2S profile at the center. No such generalization holds for $2P$ states.

The EH 2S Compton profile is observed to exhibit a secondary maximum (SM) on the low-energy transfer side. However, the intensity of this SM is reduced by an order of magnitude or more from the central peak. We discuss why we feel that these resonances have not been observed experimentally as yet, and a possible experiment to demonstrate this phenomenon is suggested. We have recently been informed that such L-shell resonance phenomenon has also been predicted in the ion-atom–scattering calculations of Nikolaev and Kruglova.[33] The position in an experimental Compton profile of such resonances can give important information on the electron spatial wave function of the atom.

We find that even when an impulse-profile calculation is done in a regime for which the impulse approximation is not really valid, the IH and EH profiles for L-shell electrons tend to cross one another in the neighborhood of the profile maximum. This leads to a strong cancellation of errors when calculating integrated Compton profiles (incoherent scattering factors). Thus we find that IH incoherent-scattering factors are observed to be extremely accurate when compared to EH incoherent-scattering factors over a wide range of incident photon energies, scattering angles, and binding energies. In cases of relatively low momentum transfer, IH incoherent-scattering factors represent a considerable improvement over conventional Waller-Hartree incoherent-scattering factors. A discussion of the errors inherent in the Waller-Hartree method of calculation is given. It is observed that when the EH incoherent-scattering factor is of the order of 0.5 or less, the Waller-Hartree result is too high by a factor of 50% or more. The L-shell calculations, as well as the earlier K-shell results, indicate that much-more-accurate incoherent-scattering factors can

TABLE VII. 2S Compton scattering with W fixed.

$(\sin\theta)/\lambda_1 = 1.2$ Å^{-1}; $Z = 5$

E_1(eV)	2θ	$(E_1/E_2^0)^2 S(EX)$
10 000	...	...
15 000	163.8°	0.976
30 000	58.5°	0.977
40 000	43.7°	0.977
60 000	28.7°	0.978

$(E_1/E_2^0) S(WH) = 0.998$

TABLE VIII. 2S Compton scattering with W fixed.

$(\sin\theta)/\lambda_1 = 0.8$ Å^{-1}; $Z = 5$

E_1(eV)	2θ	$(E_1/E_2^0)^2 S(EX)$
10 000	165.4°	0.970
15 000	82.79°	0.970
30 000	38.61°	0.971
40 000	28.70°	0.971
60 000	19.03°	0.971

$(E_1/E_2^0)^2 S(WH) = 0.999$

TABLE IX. 2S Compton scattering with W fixed.

$(\sin\theta)/\lambda_1 = 0.4$ Å^{-1}; $Z = 5$		
E_1(eV)	2θ	$(E_1/E_2^0)^2 S$(EX)
10 000	58.5°	0.492
15 000	38.6°	0.499
30 000	19.0°	0.498
40 000	14.2°	0.498
60 000	9.4°	0.497
$(E_1/E_2^0)^2 S$(WH) = 0.987		

be obtained for complex atoms at intermediate momentum transfers by direct integration of the impulse Compton profiles, rather than by using the Waller-Hartree scheme.

APPENDIX A

Symbols, definitions and abbreviations

$\hbar$ — Planck's constant divided by 2π.

m_0 — Electron mass.

e — Electron charge.

Z — Atomic number.

$Z^*(0)$ — Effective atomic number obtained by matching the impulse hydrogenic $J(0)$ and the impulse Hartree-Fock $J(0)$.

$Z^*(be)$ — Effective atomic number obtained by matching experimental binding energy using a hydrogenic model.

$a_0 \equiv \hbar^2/m_0 e^2$ — In atomic units: $a_0 = 1$.

2θ — Scattering angle.

Photon

$\vec{k}_1, \vec{k}_2$ — Incident and scattered photon wave numbers, respectively.

$\vec{k} \equiv \vec{k}_1 - \vec{k}_2$ — Scattering vector.

k — Scattering vector magnitude.

E_1, E_2 — Incident and scattered photon energies, respectively.

TABLE X. 2S Compton scattering with W fixed.

$W = 0.2$ Å^{-1}; $Z = 5$		
E_1(eV)	2θ	$(E_1/E_2^0)^2 S$(EX)
10 000	28.8°	0.074
15 000	19.0°	0.076
30 000	9.4°	0.078
40 000	7.2°	0.080
60 000	4.8°	0.065
$(E_1/E_2^0)^2 S$(WH) = 0.63		

TABLE XI. 2P Compton scattering.

$Z = 5$; $2\theta = 30°$				
E_1(eV)	S(IMP)	$S(\mathrm{EX})_{2P(0)}$	$S(\mathrm{EX})_{2P(\pm1)}$	$S(\mathrm{EX})_{av}$
5000	4.2(−3)	0.019	0.012	0.012
10 000	0.125	0.143	0.087	0.106
15 000	0.367	0.401	0.286	0.324
20 000	0.561	0.603	0.550	0.568
30 000	0.817	0.737	0.881	0.833
40 000	0.924	0.847	0.961	0.923
50 000	0.957	0.918	0.972	0.954
60 000	0.964	0.948	0.970	0.963

$E \equiv E_1 - E_2$ — Difference in incident and scattered photon energies.

$\kappa \equiv nka_0/Z$ — In atomic units:

$$\kappa^2 = \frac{10^{-6} n^2}{0.511 Z^2 \times 27.212} (E_1^2 + E_2 - 2E_1 E_2 \cos 2\theta).$$

Electron

$\vec{p}_1, \vec{p}$ — Initial- and final-electron momenta.

e_i, e_f — Initial- and final-electron energies.

$\mathfrak{K}$ — Final-electron wave number.

ψ_i, ψ_f — Initial- and final-electron wave functions.

$P \equiv n\mathfrak{K}a_0/Z$ — In atomic units:

$$P^2 = 2\left[\frac{n^2 E}{27.212\kappa Z} - \frac{1}{2}\right].$$

$q \equiv -\vec{p}_1 \cdot \vec{k}/k$ — Projection of initial-electron momentum on the scattering vector. q is related to the distance from the Compton line for scattering by a free electron. In atomic units:

$$q = \frac{nE}{27.212\kappa Z} - \frac{\kappa Z}{2n}$$

κ^0, P^0 — The values of κ and P at $q = 0$.

TABLE XII. 2P Compton scattering.

$Z = 5$; $2\theta = 90°$				
E_1(eV)	S(IMP)	$S(\mathrm{EX})_{2P(0)}$	$S(\mathrm{EX})_{2P(\pm1)}$	$S(\mathrm{EX})_{av}$
5000	0.292	0.314	0.211	0.245
10 000	0.741	0.685	0.803	0.764
15 000	0.895	0.821	0.929	0.893
20 000	0.916	0.890	0.926	0.914
30 000	0.894	0.892	0.895	0.894
40 000	0.864	0.864	0.865	0.864
50 000	0.836	0.836	0.836	0.836
60 000	0.809	0.809	0.809	0.809

Comparison of F. Bloch and our notation

F. Bloch	*In This Work*
α	$\alpha \rightarrow 2Z/na_0$
$1/\gamma$	$1/\gamma \rightarrow \kappa + P$
υ	$\upsilon \rightarrow \kappa - P$
β	$\beta \rightarrow n/2P$
	Abbreviations
EH	"Exact" hydrogenic.
IA	Impulse approximation.
IH	Impulse hydrogenic.
IHF	Impulse Hartree-Fock.

APPENDIX B

Detailed derivation of general Bloch result

We will work in the parabolic coordinates (ξ, η, φ), where

$$\xi \equiv r(1+\cos 2\theta), \quad \eta \equiv r(1-\cos 2\theta)$$

and the azimuth φ is measured around an axis in the direction of the scattering vector $\vec{\kappa}$. Thus $\vec{\kappa}\cdot\vec{r}$ in Eq. (22) becomes

$$\vec{\kappa}\cdot\vec{r} = kr\cos 2\theta = \tfrac{1}{2}k(\xi-\eta). \tag{B1}$$

The initial state (n, l, a) and the final state $(\mathfrak{K}, m, a)$ will be written as

$$|\psi_i\rangle = U_{nla}(\xi,\eta)\, e^{+ia\varphi} \tag{B2}$$

and

$$|\psi_f\rangle = U_{\mathfrak{K}ma}(\xi,\eta)\, e^{+ia\varphi} \tag{B3}$$

Now $U_{\mathfrak{K}ma}$ can be written in the form

$$U_{\mathfrak{K}ma}(\xi,\eta) = C_{\mathfrak{K}ma}(\xi\eta)^{a/2}(i\mathfrak{K})^{-2a} f_{\mathfrak{K}ma}(\xi)\, g_{\mathfrak{K}ma}(\eta), \tag{B4}$$

where we will use the well-known integrals,

$$f_{\mathfrak{K}ma}(\xi) = \frac{1}{2\pi i}\oint e^{t_1\xi}\left(t_1+\frac{i\mathfrak{K}}{2}\right)^{(a-1)/2+i(\beta+m)} \times \left(t_1-\frac{i\mathfrak{K}}{2}\right)^{(a-1)/2-i(\beta+m)} dt_1, \tag{B5}$$

TABLE XIII. $2P$ Compton scattering.

		$Z=5;\ 2\theta=180°$		
E_1(eV)	S(IMP)	$S(\mathrm{EX})_{2P^{(0)}}$	$S(\mathrm{EX})_{2P^{(\pm1)}}$	$S(\mathrm{EX})_{\mathrm{av}}$
5000	0.510	0.551	0.488	0.510
10 000	0.862	0.779	0.903	0.862
15 000	0.885	0.866	0.893	0.884
20 000	0.861	0.858	0.862	0.861
30 000	0.805	0.805	0.805	0.805
40 000	0.754	0.754	0.754	0.754
50 000	0.708	0.708	0.708	0.708
60 000	0.667	0.667	0.667	0.667

and

$$g_{\mathfrak{K}ma}(\eta) = \frac{1}{2\pi i}\oint e^{t_2\eta}\left(t_2+\frac{i\mathfrak{K}}{2}\right)^{(a-1)/2+i(\beta-m)} \times \left(t_2-\frac{i\mathfrak{K}}{2}\right)^{(a-1)/2-i(\beta-m)} dt_2, \tag{B6}$$

with $C_{\mathfrak{K}ma}$ given by

$$C_{\mathfrak{K}ma} = \tfrac{1}{2}\pi^{-3/2}\mathfrak{K}^{a+1}\, e^{\pi\beta}\,|\Gamma[(1-a)/2+i(\beta+m)]| \times|\Gamma[(1-a)/2+i(\beta-m)]|, \tag{B7}$$

where β is defined by

$$\beta \equiv Z m_0 e^2/2\hbar^2\mathfrak{K}. \tag{B8}$$

The usual representation of the continuum state is in spherical coordinates and can be written as

$$|\psi_f\rangle = (2\pi Z/\mathfrak{K}a_0)^{1/2}(1-e^{-2\pi Z/\mathfrak{K}a_0})^{-1/2}\, e^{i\vec{\kappa}\cdot\vec{r}} \times F(iZ/\mathfrak{K}a_0;\, 1;\, i(\mathfrak{K}r-\vec{\kappa}\cdot\vec{r})). \tag{B9}$$

The representation in parabolic coordinates results in a different normalization factor, which is a function of $\mathfrak{K}$ given by $C_{\mathfrak{K}ma}$. This can be seen most easily by noting that

$$|\Gamma[\tfrac{1}{2}+i(\beta\pm m)]|^2 = \pi/\cosh\pi(\beta\pm m), \tag{B10}$$

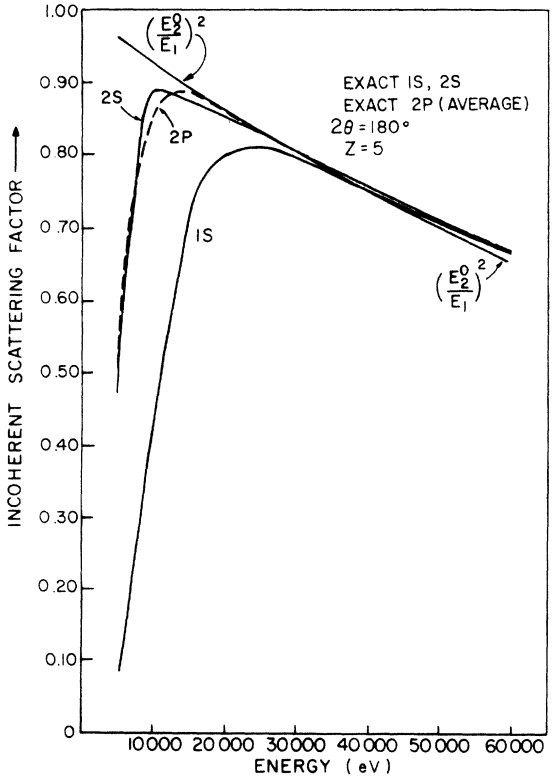

FIG. 14. Incoherent-scattering factors—variable energy.

or that

$$C_{\mathfrak{K}m}=(\mathfrak{K}/\pi^{1/2})[(1+e^{-2\pi(\beta+m)})(1+e^{-2\pi(\beta-m)})]^{-1/2}. \tag{B11}$$

Thus when we integrate $|U_{\mathfrak{K}ma}|^2$ over the domain of the parabolic quantum number $m(-\infty,+\infty)$ we will get a factor $\mathfrak{K}^2/\pi$. Therefore Eq. (26) becomes

$$I=\frac{m_0}{\hbar^2\mathfrak{K}}\left(\frac{E_2}{E_1}\right)\int_{-\infty}^{\infty}|\epsilon_{nla,\mathfrak{K}m}(k)|^2\,dm. \tag{B12}$$

In polar coordinates the initial state can be written as

$$U_{nla}=C_{nla}\,e^{-\alpha r/2}(\alpha r)^l P_l^a(\cos2\theta)L_{l+n}^{2l+1}(\alpha r), \tag{B13}$$

where

$$\alpha\equiv 2Zm_0e^2/n\hbar^2. \tag{B14}$$

Thus Eq. (28) becomes

$$\epsilon_{nla,\mathfrak{K}m}(k)=\tfrac{1}{2}\pi\int_0^{\infty}\int_0^{\infty}d\eta\,(\xi+\eta)\,e^{(ik/2)(\xi-\eta)}d\xi \times U_{\mathfrak{K}ma}(\xi,\eta)C_{nla}\,e^{-\alpha r/2}(\alpha r)^l \times P_l^a(\cos2\theta)L_{l+n}^{2l+1}(\alpha r). \tag{B15}$$

If we define $q_{la}(\mathfrak{K},m,k,t)$ as

$$q_{la}(\mathfrak{K},m,k,t)=\frac{2}{\pi}\sum_{n=1}^{\infty}\frac{\epsilon_{nla,\mathfrak{K}m}(k)}{C_{nla}(n+l)!}\,t^{n-l-1}; \tag{B16}$$

then using the expression

$$\sum_{n=1}^{\infty}L_{n+l}^{2l+1}(\alpha r)\frac{t^{n-l-1}}{(n+l)!}=\frac{(-1)^{2l+1}}{(1-t)^{2l+2}}\,e^{-\alpha rt/(1-t)}, \tag{B17}$$

in Eq. (B16), and substituting this into Eq. (B15), one gets

$$q_{la}(\mathfrak{K},m,k,t)=\int_0^{\infty}d\xi\int_0^{\infty}d\eta\,U_{\mathfrak{K}ma}(\xi,\eta)P_l^a(\cos2\theta) \times e^{(ik/2)(\xi-\eta)}(\alpha r)^l\frac{(-1)^{2l+1}}{(1-t)^{2l+2}} \times e^{-\alpha r/2-\alpha rt/(1-t)}, \tag{B18}$$

where the associated Legendre polynomials $P_l^a(\cos2\theta)$ can be written as follows:

$$P_l^a(\cos2\theta)=(1-\cos^2 2\theta)^{a/2}\sum_{j=0}^{l-a}c_j\cos^j 2\theta. \tag{B19}$$

Substituting Eqs. (B4) and (B19) into Eq. (B18), and noting that $r=(\xi+\eta)/2$ and $\cos2\theta=(\xi-\eta)/(\xi+\eta)$, we obtain

$$q_{la}(\mathfrak{K},m,k,t)=-\frac{(i\mathfrak{K})^{-2a}}{4\pi^2}\frac{\alpha^l}{2^{l-a}}C_{\mathfrak{K}ma}\frac{(-1)^{2l+1}}{(1-t)^{2l+2}}\sum_{j=0}^{l-a}c_j\int_0^{\infty}d\xi\int_0^{\infty}d\eta\,(\xi+\eta)^{1+l-a-j} \times(\xi-\eta)^j(\xi\eta)^a\exp\left[\frac{ik}{2}(\xi-\eta)-\frac{\alpha}{4}\left(\frac{1+t}{1-t}\right)(\xi+\eta)\right] \times\oint e^{t_1\xi}\left(t_1+\frac{i\mathfrak{K}}{2}\right)^{(a-1)/2+i(\beta+m)}\left(t_1-\frac{i\mathfrak{K}}{2}\right)^{(a-1)/2-i(\beta+m)}dt_1 \times\oint e^{t_2\eta}\left(t_2+\frac{i\mathfrak{K}}{2}\right)^{(a-1)/2+i(\beta-m)}\left(t_2-\frac{i\mathfrak{K}}{2}\right)^{(a-1)/2-i(\beta-m)}dt_2. \tag{B20}$$

Now one can show that

$$(\xi+\eta)^{1+l-a-j}(\xi-\eta)^j(\xi\eta)^a\exp\left[i\frac{k}{2}(\xi-\eta)-\frac{\alpha}{4}\left(\frac{1+t}{1-t}\right)(\xi+\eta)\right] =\lim_{\substack{\mu_1\to0\\ \mu_2\to0}}\left(\frac{\partial}{\partial\mu_1}+\frac{\partial}{\partial\mu_2}\right)^{1+l-a-j}\left(\frac{\partial}{\partial\mu_1}-\frac{\partial}{\partial\mu_2}\right)^j\frac{\partial^{2a}}{\partial\mu_1^a\partial\mu_2^a}\left(\exp\left\{\xi\left[t_1+\frac{ik}{2}-\frac{\alpha}{4}\left(\frac{1+t}{1-t}\right)+\mu_1\right]\right\} \times\exp\left\{\eta\left[t_2-\frac{ik}{2}-\frac{\alpha}{4}\left(\frac{1+t}{1-t}\right)+\mu_2\right]\right\}\right). \tag{B21}$$

Thus Eq. (B20) can be written as

$$q_{la}(\mathfrak{K},m,k,t)=-\frac{(i\mathfrak{K})^{-2a}}{4\pi^2}\frac{\alpha^l}{2^{l-a}}C_{\mathfrak{K}ma}\frac{(-1)^{2l+1}}{(1-t)^{2l+2}}\lim_{\substack{\mu_1\to0\\ \mu_2\to0}}\sum_{j=0}^{l-a}c_j\left(\frac{\partial}{\partial\mu_1}+\frac{\partial}{\partial\mu_2}\right)^{1+l-a-j}\left(\frac{\partial}{\partial\mu_1}-\frac{\partial}{\partial\mu_2}\right)^j\frac{\partial^{2a}}{\partial\mu_1^a\partial\mu_2^a} \times\oint dt_1\int_0^{\infty}d\xi\exp\left\{\xi\left[t_1+\frac{ik}{2}-\frac{\alpha}{4}\left(\frac{1+t}{1-t}\right)+\mu_1\right]\right\}\left(t_1+\frac{i\mathfrak{K}}{2}\right)^{(a-1)/2+i(\beta+m)}\left(t_1-\frac{i\mathfrak{K}}{2}\right)^{(a-1)/2-i(\beta+m)} \times\oint dt_2\int_0^{\infty}d\eta\exp\left\{\eta\left[t_2-\frac{ik}{2}-\frac{\alpha}{4}\left(\frac{1+t}{1-t}\right)+\mu_2\right]\right\}\left(t_2+\frac{i\mathfrak{K}}{2}\right)^{(a-1)/2+i(\beta-m)}\left(t_2-\frac{i\mathfrak{K}}{2}\right)^{(a-1)/2-i(\beta-m)} \tag{B22}$$

The integrals over ξ and η can be evaluated immediately, leaving two contour integrals over t_1 and t_2, respectively. Each of the remaining integrals has first-order poles at

$$t_1 = -\frac{ik}{2} + \frac{\alpha}{4}\left(\frac{1+t}{1-t}\right) - \mu_1, \tag{B23}$$

and at

$$t_2 = \frac{ik}{2} + \frac{\alpha}{4}\left(\frac{1+t}{1-t}\right) - \mu_2, \tag{B24}$$

and since these functions are analytic, they yield the values

$$2\pi i\left[-\frac{ik}{2} + \frac{\alpha}{4}\left(\frac{1+t}{1-t}\right) - \mu_1 + \frac{i\mathfrak{K}}{2}\right]^{(a-1)/2+i(\beta+m)}\left[-\frac{ik}{2} + \frac{\alpha}{4}\left(\frac{1+t}{1-t}\right) - \mu_1 - \frac{i\mathfrak{K}}{2}\right]^{(a-1)/2-i(\beta+m)} \tag{B25}$$

and

$$2\pi i\left[\frac{ik}{2} + \frac{\alpha}{4}\left(\frac{1+t}{1-t}\right) - \mu_2 + \frac{i\mathfrak{K}}{2}\right]^{(a-1)/2+i(\beta-m)}\left[\frac{ik}{2} + \frac{\alpha}{4}\left(\frac{1+t}{1-t}\right) - \mu_2 - \frac{i\mathfrak{K}}{2}\right]^{(a-1)/2-i(\beta-m)} \tag{B26}$$

Substituting these values into Eq. (B22), we get finally that

$$\begin{aligned} q_{la}(\mathfrak{K}, m, k, t) = (i\mathfrak{K})^{-2a}\,\frac{\alpha^l}{2^{l-a}}\,C_{\mathfrak{K}ma}\,\frac{(-1)^{2l+1}}{(1-t)^{2l+2}}\lim_{\substack{\mu_1\to 0\\ \mu_2\to 0}}\sum_{j=0}^{l-a} c_j\left(\frac{\partial}{\partial\mu_1}+\frac{\partial}{\partial\mu_2}\right)^{1+l-a-j} \\ \times\left(\frac{\partial}{\partial\mu_1}-\frac{\partial}{\partial\mu_2}\right)^{j}\frac{\partial^{2a}}{\partial\mu_1^a\,\partial\mu_2^a}\left(\frac{\alpha}{4}\,\frac{1+t}{1-t}-\mu_1-i\,\frac{(k-\mathfrak{K})}{2}\right)^{(a-1)/2+i(\beta+m)} \\ \times\left(\frac{\alpha}{4}\,\frac{1+t}{1-t}-\mu_1-i\,\frac{(k+\mathfrak{K})}{2}\right)^{(a-1)/2-i(\beta+m)}\left(\frac{\alpha}{4}\,\frac{1+t}{1-t}-\mu_2+i\,\frac{(k+\mathfrak{K})}{2}\right)^{(a-1)/2+i(\beta-m)} \\ \times\left(\frac{\alpha}{4}\,\frac{1+t}{1-t}-\mu_2+i\,\frac{(k-\mathfrak{K})}{2}\right)^{(a-1)/2-i(\beta-m)} \end{aligned} \tag{B27}$$

Evaluation of A_{nla}

The initial wave function is given by

$$|\psi_i\rangle = U_{nla}\,e^{ia\varphi} = R_{nl}(r)\,Y_{la}(2\theta,\varphi), \tag{B28}$$

where

$$R_{nl}(r) = -\left(\frac{\alpha^3}{2n}\,\frac{(n-l-1)!}{[(n+l)!]^3}\right)^{1/2} e^{-\alpha r/2} \times(\alpha r)^l\,L_{n+l}^{2l+1}(\alpha r), \tag{B29}$$

and

$$Y_{la}(2\theta,\varphi) = \left(\frac{2l+1}{4\pi}\,\frac{(l-|a|)!}{(l+|a|)!}\right)^{1/2} P_l^a(\cos 2\theta)\,e^{ia\varphi}. \tag{B30}$$

Thus we write Eq. (B28) as

$$U_{nla} = C_{nla}\,e^{-\alpha r/2}(\alpha r)^l\,P_l^a(\cos 2\theta)\,L_{n+l}^{2l+1}(\alpha r), \tag{B31}$$

where

$$C_{nla} = \left[\frac{\alpha^3}{2n}\,\frac{(n-l-1)!}{[(n+l)!]^3}\left(\frac{2l+1}{4\pi}\right)\frac{(l-|a|)!}{(l+|a|)!}\right]^{1/2}. \tag{B32}$$

From Eq. (B16)

$$\epsilon_{nla,\mathfrak{K}m}(k) = \frac{\pi}{2}\,(n+l)!\,C_{nla}\left.\frac{\partial q_{la}^{n-l-1}(\mathfrak{K}, m, k, t)}{\partial t^{n-l-1}}\right|_{t=0}, \tag{B33}$$

$$\epsilon_{nla,\mathfrak{K}m}(k) = (-1)^l\,\pi^{3/2}\,2^{3-l}\,(A_{nla})^{1/2} \times\left.\frac{\partial q_{la}^{n-l-1}(\mathfrak{K}, m, k, t)}{\partial t^{n-l-1}}\right|_{t=0}, \tag{B34}$$

then finally equating Eqs. (B33) and (B34) we get

$$A_{nla} = \frac{\alpha^3(n-l-1)!\,(2l+1)(l-|a|)!}{2^{-1-2l}\,\pi^2 n(n+l)!\,(l+|a|)!}. \tag{B35}$$

Typical values of A_{nla} are: $A_{100} = 2\alpha^3/\pi^2$; $A_{200} = \alpha^3/2\pi^2$; $A_{210} = 2\alpha^3/\pi^2$; $A_{211} = \alpha^3/\pi^2$.

APPENDIX C

Consider the integral

$$\int_{-\infty}^{\infty}\frac{z^g\,dz}{(1+e^{z-a})(1+e^{-(z+a)})}, \tag{C1}$$

where a is a constant and g is an integer. The integrand has simple poles at

$$z = a + i\pi(1+2n), \quad \text{and} \quad z = -a + i\pi(1+2n), \tag{C2}$$

where $n = 0, \pm 1, \pm 2, \ldots$.

We choose the rectangular path in Fig. 15 to

evaluate the integral in the complex plane enclosing the poles at $a+i\pi$ and at $-a+i\pi$. The contour integral around the complete rectangular path consists of the four straight-path integrals: J_1, J_2, J_3, and J_4.

Writing $z=x+iy$ and allowing J_4 to go from $x=-R$ to $x=R$, we have for the integrals J_1 and J_3

$$\int_{J_1} \frac{z^g\,dz}{(1+e^{g-a})(1+e^{-(z+a)})} = \int_0^{2\pi} \frac{(R+iy)^g\,i\,dy}{(1+e^{R-a+iy})(1+e^{-(R+a+iy)})} \tag{C3}$$

and

$$\int_{J_3} \frac{z^g\,dz}{(1+e^{a-g})(1+e^{-(z+a)})} = \int_{2\pi}^0 \frac{(-R+iy)^g\,i\,dy}{(1+e^{-R-a+iy})(1+e^{-(-R+a+iy)})} \tag{C4}$$

Taking $\lim_{|R|\to\infty}|J_1|$ and $\lim_{|R|\to\infty}|J_3|$, both of these integrals go to zero. We are left with integrals J_2 and J_4, and allowing $|R|\to\infty$ we find (writing x for R)

$$J_2 = -\int_{-\infty}^{\infty} \frac{(x+2\pi i)^g\,dx}{(1+e^{x-a})(1+e^{-(x+a)})} \tag{C5}$$

and

$$J_4 = \int_{-\infty}^{\infty} \frac{x^g\,dx}{(1+e^{x-a})(1+e^{-(x+a)})}\,. \tag{C6}$$

Evaluating the integrals at the poles, we make use of the residue theorem to obtain

$$\int_{-\infty}^{\infty} \frac{x^g\,dx}{(1+e^{x-a})(1+e^{-(x+a)})} - \int_{-\infty}^{\infty} \frac{(x+2\pi i)^g\,dx}{(1+e^{x-a})(1+e^{-(x+a)})} = 2\pi i(1-e^{-2a})^{-1}\left[(-a+i\pi)^g-(a+i\pi)^g\right]. \tag{C7}$$

To go over to the constants in Eqs. (44) and (63)

$$x=2\pi m \quad \text{and} \quad a=2\pi\beta. \tag{C8}$$

After some manipulating, and dividing through by $(2\pi)^{g+1}$, we get the desired result

$$\int_{-\infty}^{\infty} \frac{\left[m^g-(m+i)^g\right]dm}{(1+e^{-2\pi(\beta+m)})(1+e^{-2\pi(\beta-m)})} = i(1-e^{-4\pi\beta})^{-1}\left[(-\beta+\tfrac{1}{2})^g-(\beta+\tfrac{1}{2})^g\right]; \tag{C9}$$

when g is odd the value of the integral is zero, since the cosh function is even.

We may evaluate this integral by starting from $g=1$ and going to larger values of g. Thus for $g=1$,

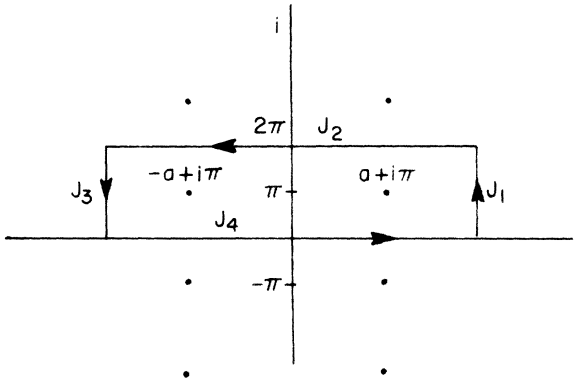

FIG. 15. Integration path to evaluate integral (C1).

$$\int_{-\infty}^{\infty} \frac{dm}{(1+e^{-2\pi(\beta+m)})(1+e^{-2\pi(\beta-m)})} = 2\beta(1-e^{-4\pi\beta})^{-1}, \tag{C10}$$

$g=3$,

$$\int_{-\infty}^{\infty} \frac{m^2\,dm}{(1+e^{-2\pi(\beta+m)})(1+e^{-2\pi(\beta-m)})} = \frac{\beta}{6}(1+4\beta^2)(1-e^{-4\pi\beta})^{-1}, \tag{C11}$$

$g=5$,

$$\int_{-\infty}^{\infty} \frac{m^4\,dm}{(1+e^{-2\pi(\beta+m)})(1+e^{-2\pi(\beta-m)})} = \frac{\beta}{5}\left(\frac{7}{24}+\frac{5\beta^2}{3}+2\beta^4\right)(1-e^{-4\pi\beta})^{-1}. \tag{C12}$$

We now want to evaluate integrals of the type

$$\int_{-\infty}^{\infty} \frac{z^g\,dz}{(1-e^{-(z+a)})(1-e^{-(a-z)})}\,, \tag{C13}$$

where again, a is a constant and g is an integer. Using the results of the integral (C9), we now make the transformation $z\to z-i\pi$. Then

$$1+e^{-(z+a)} \to 1-e^{-(z+a)}$$

$$1+e^{-(a-z)} \to 1-e^{-(a-z)},$$

resulting in

$$\int_{-\infty}^{\infty} \frac{(z-i\pi)^g-(z+i\pi)^g}{(1-e^{-(z+a)})(1-e^{-(a-z)})}\,dz = 2\pi i(1-e^{-2a})^{-1}\left[(-a+i\pi)^g-(a+i\pi)^g\right]. \tag{C14}$$

We are now in a position to evaluate the integrals in Eqs. (82) and (83). Again setting $a=2\pi\beta$ and $z=2\pi m$, we are led finally to the desired integrals

$$\int_{-\infty}^{\infty} \frac{dm}{(1-e^{-2\pi(\beta+m)})(1-e^{-2\pi(\beta-m)})} = 2\beta(1-e^{-4\pi\beta})^{-1}, \tag{C15}$$

$$\int_{-\infty}^{\infty} \frac{m^2\,dm}{(1-e^{-2\pi(\beta+m)})(1-e^{-2\pi(\beta-m)})} = -\tfrac{1}{3}\beta(1-2\beta^2)(1-e^{-4\pi\beta})^{-1}, \quad \text{(C16)}$$

$$\int_{-\infty}^{\infty} \frac{m^4\,dm}{(1-e^{-2\pi(\beta+m)})(1-e^{-2\pi(\beta-m)})} = -\tfrac{1}{15}\beta(1+10\beta^2-6\beta^4)(1-e^{-4\pi\beta})^{-1}. \quad \text{(C17)}$$

It is then just a matter of algebra to get finally

$$\int_{-\infty}^{\infty} \frac{(\beta^2-m^2)\,dm}{(1-e^{-2\pi(\beta+m)})(1-e^{-2\pi(\beta-m)})} = \tfrac{1}{3}\beta(1+4\beta^2)(1-e^{-4\pi\beta})^{-1}, \quad \text{(C18)}$$

$$\int_{-\infty}^{\infty} \frac{m^2(\beta^2-m^2)\,dm}{(1-e^{-2\pi(\beta+m)})(1-e^{-2\pi(\beta-m)})} = \tfrac{1}{15}\beta(1+5\beta^2+4\beta^4)(1-e^{-4\pi\beta})^{-1}. \quad \text{(C19)}$$

---

*Supported by Office of Naval Research Grant No. N00014-67-A-0438-001.

†Taken from the dissertation submitted in partial fulfillment of the requirements for the degree of Ph.D. in Physics.

[1]P. Eisenberger, Phys. Rev. A 5, 628 (1972).
[2]P. Eisenberger and W. A. Reed, Phys. Rev. A 5, 2085 (1972).
[3]M. Cooper and B. Williams, Philos. Mag. 22, 543 (1970).
[4]M. Cooper *et al.*, Philos. Mag. 22, 441 (1970).
[5]R. Currat, P. D. DeCicco, and R. Kaplow, Phys. Rev. B 3, 243 (1971).
[6]R. Currat, P. D. DeCicco, and R. J. Weiss, Phys. Rev. B 4, 4256 (1971).
[7]R. J. Weiss, Philos. Mag. 24, 1477 (1971).
[8]W. C. Phillips and R. J. Weiss, Phys. Rev. B 5, 755 (1972).
[9]R. J. Weiss, Philos. Mag. 25, 1511 (1972).
[10]R. H. Pratt and H. K. Tseng, Phys. Rev. A 5, 1063 (1972).
[11]P. Eisenberger and P. Platzman, Phys. Rev. A 2, 415 (1970).
[12]R. J. Weiss (private communication).
[13]L. B. Mendelsohn and F. Biggs, Phys. Rev. A 2, 688 (1972).
[14]J. W. H. Dumond, Phys. Rev. 33, 643 (1929).
[15]W. E. Duncanson and C. A. Coulson, Proc. Phys. Soc. 57, 190 (1945).
[16]R. J. Weiss, A Harvey, and W. C. Phillips, Philos. Mag. 146, 241 (1968).
[17]L. B. Mendelsohn, Frank Biggs, and J. B. Mann, Int. J. Quan. Chem. (to be published).
[18]R. Benesch and V. H. Smith, Phys. Rev. A 1, 114 (1972).
[19]R. E. Brown and V. H. Smith, Phys. Rev. A 1, 140 (1972).
[20]P. Eisenberger, W. H. Henneker, and P. Cade, J. Chem. Phys. 56, 1207 (1972).
[21]A. Gummel and M. Lax, Ann. Phys. (N.Y.) 2, 28 (1957).
[22]R. W. James, *The Optical Principles of the Diffraction of X-rays* (Cornell U. P., Itaca, N. Y., 1965), p. 110.
[23]S. Fraga and G. Malli, *Many-Electron Systems: Properties and Interactions* (Saunders, Philadelphia, 1968), p. 277.
[24]D. T. Cromer and J. B. Mann, J. Chem. Phys. 47, 1892 (1967).
[25]D. T. Cromer, Los Alamos Report No. LA-4079, 1969 (unpublished).
[26]D. E. Parks and M. Rotenberg, Phys. Rev. A 2, 521 (1972).
[27]F. Bloch, Phys. Rev. 45, 674 (1934).
[28]G. Wentzel, Z. Phys. 43, 1, 779 (1972); Z. Phys. 58, 348 (1929).
[29]L. B. Mendelsohn and F. Biggs, in *Inner-Shell Ionization Phenomena and Future Applications*, edited by R. W. Fink, S. T. Manson, J. M. Palms, and R. V. Rao (U. S. Atomic Energy Commission Conference—720404, 1973), Vol. 3, p. 1142–74.
[30]L. B. Mendelsohn and B. Bloch, Bull. Am. Phys. Soc. 17, 500 (1972).
[31]G. Cohen and N. Alexandropoulos, Solid State Commun. 10, 95 (1972).
[32]R. A. Bonham, J. Chem. Phys. 43, 1460 (1965).
[33]V. S. Nikolaev and I. M. Kruglova, Phys. Lett. A 37, 4, 315 (1971).